Clr4^{SUV39H1} and Bdf2^{BRD4} ubiquitination mediate transcriptional silencing via heterochromatic phase transitions

Hyun-Soo Kim[1], Benjamin Roche[1], Sonali Bhattacharjee[1], Leila Todeschini[2], An-Yun Chang[1], Chris Hammell[1], André Verdel[2], Robert A. Martienssen[1,3,4*]

[1] Cold Spring Harbor Laboratory, Cold Spring Harbor, New York 11724, USA.

[2] Institut for Advanced Biosciences, UMR InsermU1209/CNRS5309/UGA, University of Grenoble Alpes, Grenoble, France.

[3] Howard Hughes Medical Institute, Cold Spring Harbor Laboratory, Cold Spring Harbor, NY 11724, USA

[4] Lead Contact

* Correspondence: martiens@cshl.edu

Abstract

Heterochromatin has crucial roles in genome stability by silencing repetitive DNA and by suppressing recombination[1,2]. In the fission yeast *Schizosaccharomyces pombe*, Clr4 methylates histone H3 lysine 9 (H3K9) to maintain centromeric heterochromatin during the cell cycle, guided by RNA interference (RNAi)[3,4]. Clr4 interacts with a specialized ubiquitination complex CLRC, which is recruited in part by small RNA and the RNAi transcriptional silencing complex (RITS) but otherwise, the role of CLRC is unknown[5-8]. Here we show that the E2 ubiquitin conjugating enzyme Ubc4 interacts with CLRC and targets Clr4 for mono-ubiquitination at an intrinsically disordered region. Mono-ubiquitination is essential for the transition from co-transcriptional (H3K9me2) to transcriptional (H3K9me3) gene silencing by transiently releasing Clr4 from centromeric heterochromatin, and is reversed by the deubiquitinating enzyme Ubp3. Addition of ubiquitin changes the liquid-liquid phase separation (LLPS) of Clr4 to enhance its dynamic activity. Ubc4-CLRC also poly-ubiquitinates Bdf2, the homologue of BET family double bromodomain protein BRD4 for degradation, which otherwise accumulates at centromeres to promote transcription and production of small RNAs.

Main text

Co-transcriptional gene silencing (CTGS) depends on the production of centromeric sRNAs by RNA polymerase II and RNAi, which guides H3K9me2 restoration during S phase of cell cycle. The subsequent transition from H3K9me2 to H3K9me3 and binding of HP1 proteins Swi6 and Chp2 to heterochromatin, suppresses RNA Polymerase II-dependent transcription by transcriptional gene silencing (TGS)[2,9-11]. However, the

23 mechanism that promotes the transition from RNAi-dependent CTGS to TGS is unclear.
24 Ubiquitination is a post-translational modification which requires ubiquitin, E1 ubiquitin
25 activating enzyme, E2 ubiquitin conjugating enzyme and E3 ubiquitin ligase[12]. We
26 previously showed that a specific mutation in the E2 ubiquitin conjugating enzyme Ubc4
27 abolishes heterochromatic silencing at centromeres, mating type loci and telomeres[13]
28 (Extended Data Fig 1b, d). Overexpression of Ubc4 also causes chromosome mis-
29 segregation[14]. We found that the *ubc4-G48D* (*ubc4-1*) mutation results in Ubc4 protein
30 instability (Extended Data Fig. 1c, e). Replacement of *ubc4* with the mouse homologue
31 UBE2D2 fully complemented *ubc4-1* and *UBE2D2-G48D* had similar silencing defects
32 (Extended Data Fig. 1b). A spontaneous second-site suppressor, S137T (see Material &
33 Methods), stabilizes Ubc4-1, restoring the silencing defects (Extended Data Fig. 1d-f).

34 **Ubc4 and Cul4 regulate H3K9 methylation through RNAi**

35 The E3 ubiquitin ligase, Cul4 is also involved in heterochromatin silencing and is part of
36 the CLRC complex[5-8]. *ubc4-1* and the *cul4-GFP* fusion (*cul4-1*) mutants have very
37 similar phenotypes, including loss of silencing of *ade6*$^+$ and *ura4*$^+$ reporter genes in
38 centromeric heterochromatin (Extended Data Fig. 1b), as well as increased binding of
39 Rpb1, the catalytic component of RNA polymerase II (Extended Data Fig. 2c).
40 Interestingly, while H3K9me3 was lost from both *ubc4-1* and *cul4-1* mutants at all
41 heterochromatic loci tested, H3K9me2 had increased occupancy at *dg* and *dh* repeats.
42 Increased H3K9me2 was also observed at the centromeric *ade6*$^+$ reporter gene, which
43 accumulates small RNA, but not at the *ura4*$^+$ gene, which does not (Fig. 1a and
44 Extended Data Fig. 2a, 2b, 3a). Swi6^{HP1} protein binding was present at intermediate

45 levels, presumably because it recognizes both H3K9me2 and H3K9me3 (Extended
46 Data Fig. 2e)[9,15]. To determine whether RNAi is important for maintaining H3K9me2 in
47 *ubc4-1* mutant cells, we introduced the *ubc4-1* mutation in *dcr1Δ* mutant cells and found
48 that the *dcr1Δ ubc4-1* double mutant had greatly reduced H3K9me2, and was more
49 sensitive to microtubule destabilizing agent thiabendazole (TBZ), showing that
50 centromeric heterochromatin was completely lost (Extended Data Fig. 3b-e). The more
51 severe alleles *ubc4-3xHA* and *cul4Δ* abolished H3K9me2 altogether (Extended Data
52 Fig. 4a-c). Live imaging revealed that Ubc4 and Cul4 proteins localize to nuclear
53 periphery (Extended Data Fig. 4d), and they form a stable complex by co-
54 immunoprecipitation (Co-IP) (Extended Data Fig. 4e). Ubc4 also forms a complex with
55 Raf1 and Raf2, two other components of CLRC (Extended Data Fig. 4f). These results
56 clearly indicate that Ubc4 and Cul4 form the E2/E3 complex by which CLRC targets
57 substrates important for heterochromatin assembly.

58 **Ubc4-CLRC mono-ubiquitinates Clr4**

59 Next, we set out to identify the substrates of this novel E2/E3 complex, Ubc4-CLRC.
60 Interestingly, Clr4 co-purifies with the CLRC complex *in vivo*, but does not behave like a
61 structural component of CLRC *in vitro*[5-8]. The Clr4 human homolog, SETDB1 is mono-
62 ubiquitinated at its SET-Insertion domain and this modification is important for its H3K9
63 methyltransferase activity[16]. To test whether Clr4 is a substrate of CLRC, we purified
64 3xFlag-Clr4 protein from *S. pombe* cells (Methods) and detected a single higher
65 molecular weight form that reacted with ubiquitin antibodies in a Ubc4-dependent
66 fashion (Fig. 1c, Extended Data Fig. 5a, b). A pulldown of ubiquitinated proteins using

67 Ubiquitination Affinity Beads (UBA) revealed a similar higher molecular weight Clr4
68 which is also dependent on Ubc4 (Extended Data Fig. 5c). In addition to Ubc4, the
69 presence of this higher molecular weight Clr4 depends on Cul4, Rik1, Raf1 and Raf2,
70 the other components of CLRC but not on the proteasome inhibitor MG-132 (Extended
71 Data Fig. 5d, e). These results strongly suggest that Ubc4 together with CLRC mono-
72 ubiquitinates Clr4 *in vivo*. As the abundance of Clr4-Ub protein is too low to detect
73 ubiquitinated residues by Mass Spectrometry, we ubiquitinated 6xHis-Clr4 recombinant
74 protein purified from *E. coli* cells *in vitro*. This approach uncovered many possible
75 ubiquitination sites, which mostly reside in an intrinsically disordered region (IDR)
76 between the chromodomain (CD) and PreSET domain (Extended Data Fig. 5g-i) which
77 is involved in nucleosome binding[17]. To identify which of these were functional *in vivo*,
78 36 lysines of Clr4 were arranged into 6 subgroups, and mutated into arginines (R). We
79 also included a mutant of all 36 lysines (*AllKtoR*). The all-lysine mutant (*AllKtoR*) and
80 the second block mutant (*2-8KtoR*), corresponding to the middle of the IDR, completely
81 abolished ubiquitination (Fig. 1e and Extended Data Fig. 6b) consistent with results of
82 Mass Spectrometry. Although no single lysine to arginine mutant lost ubiquitination
83 (Extended Data Fig. 6c) we could narrow down the possible sites to 4 lysines (*clr4-2-*
84 *4KtoR*; K109, K110, K113, and K114) (Fig. 1e and Extended Data Fig. 6d-f). ChIP-Seq
85 revealed that *clr4-AllKtoR* lost both H3K9me2 and H3K9me3, resembling strong alleles
86 of *ubc4* and *cul4*, while *clr4-2-4KtoR* had the same increase of H3K9me2 and decrease
87 of H3K9me3 seen in *ubc4-1* and *cul4-1* hypomorphs (Fig. 1g and Extended Data Fig.
88 6g). Thus mono-ubiquitination of Clr4 by Ubc4-CLRC is required for H3K9 tri-
89 methylation at centromeric heterochromatin.

90 **Clr4 ubiquitination induces its dissociation from chromatin**

91 Clr4 ubiquitination does not change the histone methylation activity of Clr4 (Extended
92 Data Fig. 7a) but binding to chromatin was increased in *ubc4-1*, *cul4-1*, *clr4-2-8KtoR* or
93 *clr4-AllKtoR* mutants, especially at *dh* where sRNAs are produced (Fig. 2a and
94 Extended Data Fig. 7b). To further explore the effect of Clr4 mono-ubiquitination on
95 chromatin binding, we carried out nucleosome binding assays using *in vitro*
96 ubiquitinated 6xHis-Clr4 recombinant protein or 3xFlag-Clr4 purified from *S. pombe*
97 cells with tethered nucleosomes (Extended Data Fig. 7c). In contrast to unmodified Clr4
98 protein which had strong binding affinity to the nucleosome, especially when H3K9me3
99 was present, ubiquitinated Clr4 did not bind to the nucleosome (Fig. 2b Extended Data
100 Fig. 7d). These results are consistent with the increased binding *in vivo* in the absence
101 of mono-ubiquitination in *ubc4-1* or *cul4-1*. Binding in the absence of ubiquitin depended
102 on the Clr4 chromodomain (Fig. 2c and Extended Data Fig. 7e)[9,18]. These results
103 indicate that Clr4 mono-ubiquitination reduces the binding activity of Clr4 to chromatin
104 and that this is important for the transition from H3K9 di- to tri-methylation.

105 **Ubp3 deubiquitinates Clr4**

106 Ubiquitination is a reversible, highly dynamic and transient modification, and its removal
107 is catalyzed by deubiquitinating enzymes[12]. A deletion mutant of deubiquitinating
108 enzyme Ubp3 rescues heterochromatic silencing defects of *ago1Δ,* and *ubp3Δ* shows
109 positive epistatic genetic interactions with CLRC component mutants[19,20]. While deletion
110 of Ubp3 did not increase Clr4 mono-ubiquitination (Extended Data Fig. 8a),
111 overexpression had a silencing defect at the centromeric *ura4*$^{+}$ reporter gene and

112 reduced the mono-ubiquitination of Clr4 (Fig. 1f and Extended Data Fig. 8b). The
113 overexpression of Ubp3 also resulted in an increase of H3K9me2 and decrease of
114 H3K9me3 as well as increased RNA Pol II binding, noncoding RNA transcription and
115 Clr4 binding at centromeric heterochromatin (Fig. 1g and Extended Data Fig. 8c-f).
116 These results indicate that Ubp3 counteracts Clr4 mono-ubiquitination activity of Ubc4-
117 CLRC and reverses Clr4 activity.

118 **Clr4^{IDR} displays ubiquitin-dependent phase separation properties.**

119 Swi6 forms 4 foci in the nucleus corresponding to the chromocenter and the three
120 telomeric clusters, all of which depend on Clr4 (Fig. 3a and Extended Data Fig. 9a). In
121 *ubc4-1* mutants, the telomeric foci disappear and the chromocenter is retained, while in
122 *dcr1Δ* mutants the telomeric foci are retained and the chromocenter is reduced (Fig. 1b
123 and 3a and Extended Data Fig. 3c, 3d and 9a). Along with HP1 proteins from human,
124 Swi6 has been shown to undergo liquid-liquid phase separation (LLPS) which
125 contributes to the highly dynamic features of heterochromatin[21,22]. Clr4 protein has an
126 intrinsically disordered region (IDR) or low-complexity domain (LCD) between its
127 chromodomain (CD) and PreSET domain[17], and IDR/LCD are domains typically
128 responsible for phase separation (Extended Data Fig. 9b)[23]. We found that recombinant
129 GFP-Clr4^{Full} and GFP-Clr4^{IDR} (51-220 amino acids) proteins form liquid droplets *in vitro*
130 at low salt conditions even without addition of crowding agents like PEG8000 (Fig. 3b
131 and Extended Data Fig. 9c, d). Next, we treated the proteins with 1,6-Hexanediol which
132 dissolves liquid droplets by disrupting hydrophobic interaction of protein-protein or
133 protein-RNA[24]. We found that the formation of liquid droplets of GFP-Clr4^{IDR} was greatly

134 reduced by 1,6-haxanediol treatment indicating that these liquid droplets are formed by
135 LLPS (Extended Data Fig. 9d). Clr4^{IDR} binds ubiquitin[25] and we added concentrated
136 ubiquitin to GFP-Clr4^{IDR} in order to mimic the effect of ubiquitination of Clr4. Strikingly,
137 we found that adding ubiquitin greatly reduced the size of LLPS of GFP-Clr4^{IDR} (Fig. 3b,
138 c). Furthermore, fluorescence recovery after photobleaching (FRAP) of the liquid
139 droplets showed a faster recovery rate of GFP-Clr4^{IDR} with ubiquitin than GFP-Clr4^{IDR}
140 alone (Fig. 3d, Extended Data Fig. 9e) indicating that increased dynamics of GFP-
141 Clr4^{IDR} by addition of ubiquitin confer reduced size of liquid droplets and escape from
142 the LLPS.

143 **Ubc4 and Cul4 regulate transcription of sRNA through Bdf2^{BRD4}**

144 In *ubc4-1* and *cul4-1* mutants, we observed an almost 2-fold increase of centromeric
145 sRNA, as previously observed for *cul4* (Fig. 4a, Extended Data Fig. 10a)[18],
146 accompanied by increased chromatin binding of Ago1 and Chp1, two other components
147 of the RNA-induced transcriptional gene silencing (RITS) complex (Extended Data Fig.
148 10c). The putative H3K9 demethylase, Epe1, localizes to centromeric heterochromatin
149 in a Swi6-dependent manner and contributes to sRNA production[26,27]. The BET family
150 double bromodomain protein Bdf2 binds to the centromeric heterochromatin boundary
151 in Epe1-dependent manner and interacts with the TFIID transcription factor
152 complex[28,29]. *bdf2Δ* suppressed the increased sRNA production in *ubc4-1* and *cul4-1*
153 mutant cells (Fig. 4a). The chromatin binding of Bdf2 at centromeric heterochromatin
154 was greatly increased in both *ubc4-1* and *cul4-1* (Fig. 4b) and at euchromatic genes in
155 *ubc4-1* (Extended Data Figure 10d, e), while the protein level was increased in *ubc4-1*

156 only (Fig. 4c). These results suggest that Ubc4 is a general regulator for Bdf2, while
157 Cul4 regulates Bdf2 specifically at centromeric heterochromatin. Bdf2 protein purified
158 from cells treated with proteasome inhibitor MG-132 accumulated multiple ubiquitinated
159 bands dependent on Ubc4, suggesting that Ubc4 poly-ubiquitinates Bdf2 for its
160 degradation (Fig. 4d). These results indicate that Ubc4 and Cul4 regulates the protein
161 level and chromatin binding of Bdf2 by poly-ubiquitination, which is important for sRNA
162 production by recruiting TFIID and RNA Pol II to centromeric heterochromatin.

163 **Discussion**

164 We demonstrate that Ubc4-CLRC is essential for the switch between RNAi-dependent
165 CTGS and RNAi-independent TGS (Fig. 4e). During S phase, centromeric
166 heterochromatin is transcribed, and CLRC is recruited to centromeric heterochromatin
167 by the RITS complex and small RNA[10,11,30]. Clr4 di-methylates newly deposited H3K9,
168 and has strong binding affinity to existing H3K9me3. Subsequent mono-ubiquitination of
169 Clr4 by Ubc4-CLRC releases it from H3K9me3, allowing tri-methylation of adjacent
170 H3K9me1 or -me2 nucleosomes independent of RNAi[31]. Mono-ubiquitination also
171 triggers dissolution of subcellular phase separated droplets, allowing replacement by
172 Swi6 condensates that also bind H3K9me3 and silence transcription[22]. Poly-
173 ubiquitination of Bdf2 further reduces transcription and small RNA production
174 completing the transition to TGS. De-ubiquitination by Ubp3 reverses the process and
175 allows Clr4 recruitment in the next cell cycle (Fig. 4e).

176 In *ubc4-1* and *cul4-1* mutants, or in mutants of Clr4 that can no longer be ubiquitinated,
177 CTGS cannot transition to TGS, leading to increased sRNA production, and failure to
178 release Clr4. In contrast, strong *ubc4-3xHA* and *cul4Δ* mutants completely abolish
179 centromeric heterochromatin resembling *clr4Δ*, *rik1Δ*, *raf1Δ* and *raf2Δ* (Extended Data
180 Fig. 4a-c), because Clr4 is no longer recruited to heterochromatin by CLRC and RNAi in
181 the first place (Extended Data Fig. 5f). Ubc4-CLRC may possess additional targets,
182 such as H3K14, which was recently shown to be a prerequisite for H3K9 methylation *in*
183 *vitro*[25]. Bdf2, like its human homologue BRD4, has IDRs which may induce LLPS of
184 acetylated chromatin (Extended Data Fig. 9f)[32]. Poly-ubiquitination of Bdf2 may similarly
185 release Bdf2 from the heterochromatin phase for subsequent degradation[33]. The
186 ubiquitin-related protein modifier SUMO contributes to small RNA-dependent
187 localization of the Clr4 homologue SETDB1 to chromatin in Drosophila[34], and is
188 required for heterochromatic silencing in *S. pombe*[35], which we speculate may also be
189 mediated by a similar mechanism as reported here[36]. The existence of IDR/LCD
190 between chromo and PreSET domains of mammalian SUV39H1 (Extended Data Fig.
191 9g) and the interaction of human BRD4 with CUL4B[37] suggest that parallel mechanisms
192 might regulate transcriptional silencing in higher eukaryotes.

References

1 Janssen, A., Colmenares, S. U. & Karpen, G. H. Heterochromatin: Guardian of the Genome. *Annu Rev Cell Dev Biol* **34**, 265-288, doi:10.1146/annurev-cellbio-100617-062653 (2018).

2 Castel, S. E. & Martienssen, R. A. RNA interference in the nucleus: roles for small RNAs in transcription, epigenetics and beyond. *Nat Rev Genet* **14**, 100-112, doi:10.1038/nrg3355 (2013).

3 Volpe, T. A. *et al.* Regulation of heterochromatic silencing and histone H3 lysine-9 methylation by RNAi. *Science* **297**, 1833-1837, doi:10.1126/science.1074973 (2002).

4 Verdel, A. *et al.* RNAi-mediated targeting of heterochromatin by the RITS complex. *Science* **303**, 672-676, doi:10.1126/science.1093686 (2004).

5 Horn, P. J., Bastie, J. N. & Peterson, C. L. A Rik1-associated, cullin-dependent E3 ubiquitin ligase is essential for heterochromatin formation. *Genes Dev* **19**, 1705-1714, doi:10.1101/gad.1328005 (2005).

6 Hong, E. J., Villén, J., Gerace, E. L., Gygi, S. P. & Moazed, D. A cullin E3 ubiquitin ligase complex associates with Rik1 and the Clr4 histone H3-K9 methyltransferase and is required for RNAi-mediated heterochromatin formation. *RNA Biol* **2**, 106-111, doi:10.4161/rna.2.3.2131 (2005).

7 Jia, S., Kobayashi, R. & Grewal, S. I. Ubiquitin ligase component Cul4 associates with Clr4 histone methyltransferase to assemble heterochromatin. *Nat Cell Biol* **7**, 1007-1013, doi:10.1038/ncb1300 (2005).

215 8 Kuscu, C. *et al.* CRL4-like Clr4 complex in Schizosaccharomyces pombe
216 depends on an exposed surface of Dos1 for heterochromatin silencing. *Proc Natl*
217 *Acad Sci U S A* **111**, 1795-1800, doi:10.1073/pnas.1313096111 (2014).
218 9 Jih, G. *et al.* Unique roles for histone H3K9me states in RNAi and heritable
219 silencing of transcription. *Nature* **547**, 463-467, doi:10.1038/nature23267 (2017).
220 10 Kloc, A., Zaratiegui, M., Nora, E. & Martienssen, R. RNA interference guides
221 histone modification during the S phase of chromosomal replication. *Curr Biol* **18**,
222 490-495, doi:10.1016/j.cub.2008.03.016 (2008).
223 11 Chen, E. S. *et al.* Cell cycle control of centromeric repeat transcription and
224 heterochromatin assembly. *Nature* **451**, 734-737, doi:10.1038/nature06561
225 (2008).
226 12 Hochstrasser, M. Origin and function of ubiquitin-like proteins. *Nature* **458**, 422-
227 429, doi:10.1038/nature07958 (2009).
228 13 Irvine, D. V. *et al.* Mapping epigenetic mutations in fission yeast using whole-
229 genome next-generation sequencing. *Genome Res* **19**, 1077-1083,
230 doi:10.1101/gr.089318.108 (2009).
231 14 Javerzat, J. P., Cranston, G. & Allshire, R. C. Fission yeast genes which disrupt
232 mitotic chromosome segregation when overexpressed. *Nucleic Acids Res* **24**,
233 4676-4683, doi:10.1093/nar/24.23.4676 (1996).
234 15 Schalch, T. *et al.* High-affinity binding of Chp1 chromodomain to K9 methylated
235 histone H3 is required to establish centromeric heterochromatin. *Mol Cell* **34**, 36-
236 46, doi:10.1016/j.molcel.2009.02.024 (2009).

237 16 Sun, L. & Fang, J. E3-Independent Constitutive Monoubiquitination
238 Complements Histone Methyltransferase Activity of SETDB1. *Mol Cell* **62**, 958-
239 966, doi:10.1016/j.molcel.2016.04.022 (2016).
240 17 Akoury, E. *et al.* Disordered region of H3K9 methyltransferase Clr4 binds the
241 nucleosome and contributes to its activity. *Nucleic Acids Res* **47**, 6726-6736,
242 doi:10.1093/nar/gkz480 (2019).
243 18 Zhang, K., Mosch, K., Fischle, W. & Grewal, S. I. Roles of the Clr4
244 methyltransferase complex in nucleation, spreading and maintenance of
245 heterochromatin. *Nat Struct Mol Biol* **15**, 381-388, doi:10.1038/nsmb.1406
246 (2008).
247 19 Reyes-Turcu, F. E., Zhang, K., Zofall, M., Chen, E. & Grewal, S. I. Defects in
248 RNA quality control factors reveal RNAi-independent nucleation of
249 heterochromatin. *Nat Struct Mol Biol* **18**, 1132-1138, doi:10.1038/nsmb.2122
250 (2011).
251 20 Ryan, C. J. *et al.* Hierarchical modularity and the evolution of genetic
252 interactomes across species. *Mol Cell* **46**, 691-704,
253 doi:10.1016/j.molcel.2012.05.028 (2012).
254 21 Larson, A. G. *et al.* Liquid droplet formation by HP1α suggests a role for phase
255 separation in heterochromatin. *Nature* **547**, 236-240, doi:10.1038/nature22822
256 (2017).
257 22 Sanulli, S. *et al.* HP1 reshapes nucleosome core to promote phase separation of
258 heterochromatin. *Nature* **575**, 390-394, doi:10.1038/s41586-019-1669-2 (2019).

259 23 Kato, M. *et al.* Cell-free formation of RNA granules: low complexity sequence
260 domains form dynamic fibers within hydrogels. *Cell* **149**, 753-767,
261 doi:10.1016/j.cell.2012.04.017 (2012).
262 24 Kroschwald, S. *et al.* Promiscuous interactions and protein disaggregases
263 determine the material state of stress-inducible RNP granules. *Elife* **4**, e06807,
264 doi:10.7554/eLife.06807 (2015).
265 25 Oya, E. *et al.* H3K14 ubiquitylation promotes H3K9 methylation for
266 heterochromatin assembly. *EMBO Rep* **20**, e48111,
267 doi:10.15252/embr.201948111 (2019).
268 26 Zofall, M. & Grewal, S. I. Swi6/HP1 recruits a JmjC domain protein to facilitate
269 transcription of heterochromatic repeats. *Mol Cell* **22**, 681-692,
270 doi:10.1016/j.molcel.2006.05.010 (2006).
271 27 Trewick, S. C., Minc, E., Antonelli, R., Urano, T. & Allshire, R. C. The JmjC
272 domain protein Epe1 prevents unregulated assembly and disassembly of
273 heterochromatin. *Embo j* **26**, 4670-4682, doi:10.1038/sj.emboj.7601892 (2007).
274 28 Wang, J. *et al.* Epe1 recruits BET family bromodomain protein Bdf2 to establish
275 heterochromatin boundaries. *Genes Dev* **27**, 1886-1902,
276 doi:10.1101/gad.221010.113 (2013).
277 29 Kim, H. S. *et al.* Identification of a BET family bromodomain/casein kinase II/TAF-
278 containing complex as a regulator of mitotic condensin function. *Cell Rep* **6**, 892-
279 905, doi:10.1016/j.celrep.2014.01.029 (2014).

280 30 Bayne, E. H. *et al.* Stc1: a critical link between RNAi and chromatin modification
281 required for heterochromatin integrity. *Cell* **140**, 666-677,
282 doi:10.1016/j.cell.2010.01.038 (2010).
283 31 Al-Sady, B., Madhani, H. D. & Narlikar, G. J. Division of labor between the
284 chromodomains of HP1 and Suv39 methylase enables coordination of
285 heterochromatin spread. *Mol Cell* **51**, 80-91, doi:10.1016/j.molcel.2013.06.013
286 (2013).
287 32 Gibson, B. A. *et al.* Organization of Chromatin by Intrinsic and Regulated Phase
288 Separation. *Cell* **179**, 470-484.e421, doi:10.1016/j.cell.2019.08.037 (2019).
289 33 Yasuda, S. *et al.* Stress- and ubiquitylation-dependent phase separation of the
290 proteasome. *Nature* **578**, 296-300, doi:10.1038/s41586-020-1982-9 (2020).
291 34 Ninova, M. *et al.* Su(var)2-10 and the SUMO Pathway Link piRNA-Guided Target
292 Recognition to Chromatin Silencing. *Mol Cell* **77**, 556-570.e556,
293 doi:10.1016/j.molcel.2019.11.012 (2020).
294 35 Xhemalce, B., Seeler, J. S., Thon, G., Dejean, A. & Arcangioli, B. Role of the
295 fission yeast SUMO E3 ligase Pli1p in centromere and telomere maintenance.
296 *Embo j* **23**, 3844-3853, doi:10.1038/sj.emboj.7600394 (2004).
297 36 Shin, J. A. *et al.* SUMO modification is involved in the maintenance of
298 heterochromatin stability in fission yeast. *Mol Cell* **19**, 817-828,
299 doi:10.1016/j.molcel.2005.08.021 (2005).
300 37 Liu, H. *et al.* Inflammation-dependent overexpression of c-Myc enhances
301 CRL4(DCAF4) E3 ligase activity and promotes ubiquitination of ST7 in colitis-
302 associated cancer. *J Pathol* **248**, 464-475, doi:10.1002/path.5273 (2019).
303

304 ## Materials and Methods

305 **Yeast strains and plasmids manipulation**

306 Yeast strains, oligonucleotide sequences and plasmids are listed in Supplementary
307 Information Table S1-3. All yeast strains were constructed by PCR-based targeting
308 method[38] and lithium acetate transformation method[39]. For N-terminus tagging of 3xFlag
309 to *clr4*, *rik1* and *raf1*, endogenous promoters and terminators of each gene were used.
310 For some 3xFlag-Clr4 lysine mutants, *adh1* terminator with Kan resistant (Kan^R) gene
311 was inserted at the end of *clr4* open reading frames (ORF). For overexpression of *ubp3*
312 and *ubp8*, 500 bp of *adh1* promoter was inserted between their promoter and ORF. To
313 construct pET-14b-Clr4, the coding DNA sequence of full-length Clr4 (amino acids 1-
314 490) was amplified from *S. pombe* genomic DNA, digested with *NdeI* and cloned into
315 *NdeI*-digested pET-14b. For pHis-parallel-GFP-$Clr4^{Full}$ or pHis-parallel-GFP-$Clr4^{IDR}$
316 construction, the coding DNA sequence of full-length $Clr4^{Full}$ (amino acids 1-490) or
317 $Clr4^{IDR}$ (amino acids 51-220) were amplified from *S. pombe* genomic DNA, digested
318 with *BamHI*/*XhoI* and cloned into *BamHI*/*XhoI*-digested pHis-parallel-GFP.

319 **Chromatin Immunoprecipitation (ChIP)**

320 Chromatin Immunoprecipitation (ChIP) experiments were performed as previously
321 described[29]. Briefly, freshly grown 40 ml cells in YES were fixed with 1% formaldehyde
322 from 37% stock (Sigma F8775) for 20 min at room temperature for H3K9me2,
323 H3K9me3, RNA Pol II, Ago1 and Chp1 ChIP. For Swi6 and 3xFlag-Clr4 ChIP, 40 ml
324 cells were pre-incubated at 18 °C for 2 h and fixed with 1.45% Formaldehyde from 16%
325 stock (ThermoFisher 28908) for 30 min at 18 °C. Cells were quenched with 360 mM

326 glycine and 2.4 mM Tris for 5 min. Whole-cell extracts (WCE) were prepared using
327 FastPrep-24 and sonicated using Covaris. 1~2 µg of antibodies like anti-H3K9me2
328 (Abcam ab1220), anti-H3K9me3 (Absolute Antibody Ab00700-1.26), anti-RNA
329 polymerase II (BioLegend 904001), Swi6 (Abcam ab188276), Ago1 (Abcam Ab18190),
330 Chp1 (Abcam ab18191) and anti-Flag (Sigma F1804) were pre-incubated with 50 µl
331 Protein A and Protein G sepharose (GE 17513801 and 17061801) mix for 3~4 h and
332 then incubated with sheared chromatin overnight at 4 °C. After washing, bead-antibody-
333 chromatin mixture were treated with Proteinase K (ThermoFisher 100005393) for 1 h
334 ant 42 °C and incubated 5~6 h at 65 °C to reverse cross-links. DNA was cleaned up
335 using ChIP DNA Clean & Concentrator (Zymo Research D5205) and subsequently used
336 for qPCR or ChIP-Seq.

337 **ChIP-Seq**

338 ChIP-Seq libraries were constructed using NEBNext Ultra II DNA Library Prep Kit for
339 Illumina (NEB E7645) and barcoded multiplex libraries were sequenced using Illumina
340 MiSeq platform, which generates paired-end 101 bp reads. Raw reads were trimmed
341 using Trimmomatic, mapped to *S. pombe* genome using Bowtie2 and visualized in IGV
342 genome browser. Total ChIP-seq read counts for defined region were analyzed using
343 MultiBigwigSummary or MultiBamSummary.

344 **Co-Immunoprecipitation (Co-IP) and Immunoprecipitation (IP) for ubiquitinated**
345 **Clr4**

346 Whole-cell extracts (WCE) were prepared from freshly grown yeast cells in lysis buffer

347 (40mM Tris-HCl, pH 7.5, 1 mM EDTA, 10% Glycerol, 0.1% NP-40, 300 mM NaCl) with
348 Protease inhibitor cocktail (Roche 11836170001). For Co-IP of Cul4-GFP with Ubc4, 2
349 μg of GFP antibody (Roche 11814460001) was pre-incubated with 50 μl Protein A and
350 Protein G Sepharose (GE Healthcare 17513801 and 17061801) mix for 3~4 h and then
351 incubated with WCE overnight at 4 °C. After washing, purified proteins were loaded on
352 4–20% Mini-PROTEAN TGX Gel (Bio-rad 456-1093) and Western blotting was
353 performed with anti-GFP (Abcam 290) and anti-mUBE2D3 (Proteintech 11677-1-AP)
354 antibodies to detect Cul4-GFP and Ubc4 using ECL (Thermo Fisher 32209) assay
355 according to the manufacturer's instruction. For Co-IP of Flag-Rik1, Flag-Dos1 or Dos2-
356 Flag with Ubc4, 50 μl of Anti-Flag M2 Affinity Gel (Sigma A2220) was incubated with
357 WCE overnight at 4 °C. For detection of Flag tagged protein and Ubc4, anti-Flag (Sigma
358 F7425) and anti-mUBE2D3 (Proteintech 11677-1-AP) antibodies were used. For
359 Immunoprecipitation of ubiquitinated Clr4, WCE prepared from freshly grown cells in
360 lysis buffer (50mM Hepes, pH 7.6, 150mM NaCl, 300mM KAc, 5mM MgAc, 10%
361 Glycerol, 20mM β-GP, 1mM EDTA, 1mM EGTA, 0.1% NP-40, 1mM DTT, 250U/ml
362 Dnase I (Roche 04716728001), 25~50 μg/ml Rnase A (Sigma R4642), 1mM PMSF,
363 0.3mM PR-619 (Sigma 662141)) with Protease inhibitor cocktail (Roche 11836170001)
364 and De-ubiquitination/sumoylation Inhibitor (Cytoskeleton NEM09BB) was incubated
365 with Anti-Flag M2 Affinity Gel or Ubiquitination Affinity Beads (UAB, Cytoskeleton
366 UBA01- Beads) overnight at 4 °C. For detection of ubiquitinated Clr4 protein, anti-Flag
367 (Sigma F7425) or anti-ubiquitin (Cell Signalling 3936T) antibodies were used. Cells
368 were also treated with proteasome inhibitor 100 μM MG-132 (APExBIO A2585) for 4 h
369 before harvesting.

370 **Quantitative reverse transcription PCR (RT-qPCR)**

371 Total RNAs were purified from freshly grown yeast cells using *Quick*-RNA
372 Fungal/Bacterial Miniprep Kit (Zymoresearch R2014). Genomic DNAs were removed
373 using DNase I (Roche 04716728001) and RNAs were cleaned using RNA Clean &
374 Concentrator (Zymoresearch R1013). Reverse transcription was carried out using
375 SuperScript IV First-Strand Synthesis System (ThermoFisher 18091050) with random
376 hexamer or oligo dT as primers. For quantitative PCR (qPCR), iQ SYBR Green
377 Supermix (Bio-rad 1708882) was used with the primers listed in Supplementary
378 Information Table 2 and samples were run on CFX96 Real-Time PCR Detection System
379 (Bio-rad).

380 **sRNA-Seq**

381 Total RNAs were purified from freshly grown yeast cells using *Quick*-RNA
382 Fungal/Bacterial Miniprep Kit (Zymoresearch R2014) and sRNA were enriched using
383 RNA Clean & Concentrator (Zymoresearch R1013). sRNA libraries were constructed
384 using NEBNext Small RNA Library Prep Set for Illumina (NEB E7330) and barcoded
385 multiplex libraries were sequenced using Illumina MiSeq platform, which generates
386 single-end 36 nt reads. Reads were adapter-trimmed using FASTX-Toolkit, keeping a
387 minimum read size of 15 nt, and mapped to the *S. pombe* genome using Bowtie[40]
388 allowing up to 1 mismatch. The strand-specific genomic coverage was calculated using
389 Bedtools[41] and represented in 20 nt windows.

390 **Silencing spot assay**

391 Cells grown freshly on YES plate were picked and resuspended in water to make a
392 concentration of ~5 × 10^4 cells per µl. 8 µl of 10-fold serial dilutions were spotted on
393 appropriate plates like YES, YE, EMM-Ura, YES+FOA, YES+TBZ, and incubated 3
394 days at 30 °C for photography. *ura4*$^+$ reporter gene silencing was also tested on 5-
395 fluoro-orotic acid (FOA) plates, which kills cells expressing Ura4.

396

397 **Iodine staining**

398 Freshly grown yeast cells were spotted on SPA plates to induce sporulation, incubated
399 at room temperature for 3 days, and then stained with iodine vapor for 2-3 min. Staining
400 of starch which is abundant in mature spore produces a dark brown color.

401 **EMS mutagenesis and whole-genome sequencing for *ubc4-G48D suppressor***

402 EMS mutagenesis was carried out as previously described[42]. Briefly, freshly grown 1 x
403 10^9 yeast cells were washed with distilled water, resuspended in 1.5 ml of 0.1 M sodium
404 phosphate buffer (pH 7.0) and treated with 50 µl EMS (Sigma M0880) for 1h at 30 °C.
405 0.2 ml of treated cells was moved to 8 ml of sterile 5% sodium thiosulfate to inactivate
406 EMS. Cells were washed, resuspended in sterile water and plated on YES plate. Single
407 colonies from plates were patched on SPA plates to induce sporulation, incubated at
408 room temperature for 3 days, and then stained with iodine vapor for 2-3 min. For whole-
409 genome sequencing for *ubc4-G48D* suppressors, genomic DNA was purified from
410 freshly grown yeast cells using Genomic-tip 20/G column (QIAGEN 10223). DNA library
411 was constructed using the TruSeq DNA PCR-Free Library Prep Kit (Illumina 20015962).

412 Barcoded DNA library was sequenced using Illumina MiSeq platform, which generates
413 paired-end 151 nt reads and analyzed as previously described[43]. Briefly, reads were
414 adapter-trimmed and quality-filtered using Sickle (paired-end mode), then mapped to
415 the *S. pombe* genome using Bowtie2[44]. Duplicate reads were removed using Samtools
416 (≤ 0.14% per library). SNPs were called using FreeBayes to find SNPs present in
417 suppressor strain but absent in the parental strain[45]. This uncovered a G→C
418 transversion at position chr2:716192, a second-site mutation in the *ubc4* gene. The
419 mutation was verified by Sanger sequencing and confirmed by constructing fresh same
420 mutation.

421 **Live cell imaging**

422 Images of freshly growing cells were collected using Zeiss Axio Imager M2 with DIC and
423 EGFP channels and processed using Zeiss Zen software.

424 **CLRC complex purification from *S. pombe***

425 Protein purifications were performed as described previously[4]. Briefly, Rik1-TAP were
426 purified from 6 to 12 g of cells. Cells were lysed in 1 volume of lysis buffer (50 mM
427 HEPES-KOH, pH 7.6, 300 mM KAc, 10% glycerol, 1 mM EGTA, 1 mM EDTA, 0.1% NP-
428 40, 1 mM DTT, 5 mM MgAc, 1 mM NaF, 20 mM β-GP, 1 mM PMSF, 1 mM Benzamidine
429 and 1 µg/ml of Leupeptin, Aprotinin, Bestatin and Pepstatin). 1 volume lysis buffer was
430 added and the lysate was centrifuged at 16,500 rpm for 25 min at 4 °C in a SA600 rotor.
431 The first affinity purification was performed using Ig-G Sepharose beads at 4 °C for 2 h.
432 The beads were washed with lysis buffer and TEV-C buffer (10 mM Tris-HCl, pH 8.0,

433 150 mM KAc, 0.1% NP-40, 0.5 mM EDTA, 1 mM DTT) and bound protein was eluted
434 using a GST-TEV protease. The eluate was diluted in 2 volumes of CAM-B buffer (10
435 mM Tris-HCL, pH 8.0, 150 mM NaCl, 1 mM MgAc, 1 mM Imidazole, 2 mM $CaCl_2$, 10
436 mM βME) and the second affinity purification was performed by adding Calmodulin-
437 Sepharose at 4 °C for 1 h. The beads lysate was washed with CAM-B buffer containing
438 0.1 % NP-40 and bound protein was eluted with CAM-E buffer (10 mM Tris-HCL, pH
439 8.0, 150 mM NaCl, 1 mM MgAc, 1 mM Imidazole, 10 mM EGTA, 10 mM βME).

440 **Recombinant protein purification from *E. coli*, *in vitro* ubiquitination, Histone**
441 **Methylation assay and nucleosome binding assay**
442 BL21-CodonPlus (DE3)-RIL strains (Agilent Technologies 230245) that express 6xHis-
443 Clr4, 6xHis-GFP-Clr4^{Full} or 6xHis-GFP-Clr4^{IDR} were grown with 0.4 mM IPTG for 20 h at
444 18 °C. Induced proteins were purified on HisPur Ni-NTA Superflow Agarose
445 (ThermoFisher 25214) and eluted with elution buffer containing 150 mM Imidazole. For
446 *in vitro* ubiquitination, purified 6xHis-Clr4 protein was mixed with human Ubiquitin-
447 activating Enzyme (UBE1, R&D systems E-305), human UbcH5c/UBE2D3 (R&D
448 systems E2-627), human Ubiquitin (R&D systems U-100H) or human HA-Ubiquitin
449 (R&D systems U-110), Mg-ATP (R&D systems B-20) and 10x E3 Ligase Reaction
450 Buffer (R&D systems B-71). Addition of Rik1-TAP complex purified from *S. pombe* also
451 added to the reaction gave similar results. For Histone Methylation assay, ubiquitinated
452 or unmodified Clr4 proteins were mixed with Recombinant Mononucleosomes (H3.1,
453 Active Motif 31467) or Recombinant Mononucleosomes H3K9me3 (H3.2, Active Motif
454 31555) and *S*-(5′-Adenosyl)-*L*-methionine chloride dihydrochloride (SAM, Sigma 7007)

455 in HMT buffer (50mM Tris, pH 8.0, 10 mM $MgCl_2$, 1 mM DTT, 5% Glycerol and 1 mM
456 PMSF). Samples were boiled and loaded on 4–20% Mini-PROTEAN TGX Gel (Bio-rad
457 456-1093) and Western blotting was performed with anti-His (ThermoFisher MA1-135),
458 anti-HA (Roche 11583816001), anti-H3 (Abcam ab1791), and anti-H3K9me3 (Abcam
459 ab8898) using ECL (Thermo Fisher 32209) assay according to the manufacturer's
460 instruction. For nucleosome binding assay, biotin labeled Recombinant
461 Mononucleosomes (H3.1, Active Motif 31467) or Recombinant Mononucleosomes
462 H3K9me3 (H3.2, Active Motif 31555) was pre-incubated with Streptavidin beads (GE
463 Healthcare 17-5113-01) and incubated in vitro ubiquitinated Clr4 or Clr4 proteins
464 purified from *S. pombe* cells. Samples were boiled and loaded on 4–20% Mini-
465 PROTEAN TGX Gel (Bio-rad 456-1093) and Western blotting was performed with anti-
466 Flag (Abcam ab1791), anti-H3K9me3 (Abcam ab8898) and anti-H3 (Abcam ab1791),
467 and using ECL (Thermo Fisher 32209) assay according to the manufacturer's
468 instruction.

469 **Mass Spectrometry**

470 The gel band sample was reduced and alkylated with *N*-ethylmaleimide (NEM),
471 digested with trypsin for 1.5 h at 37 °C and washed with ammonium
472 bicarbonate/acetonitrile to remove stain, SDS and other reagents. Peptides were
473 extracted from the gel pieces, dried down and re-dissolved in 2.5% acetonitrile, 0.1%
474 formic acid. Each digest was run by nanoLC-MS/MS using a 2 h gradient on a 0.075
475 mm x 250 mm C18 column feeding into a Q-Exactive HF mass spectrometer. All
476 MS/MS samples were analyzed using Mascot (Matrix Science, London, UK; version

477 2.6.1). Mascot was set up to search the cRAP_20150130.fasta;
478 custom4_20190215.fasta; SwissProt_2019_02 database (selected for
479 *Schizosaccharomyces pombe*, unknown version, 5269 entries) assuming the digestion
480 enzyme trypsin. Mascot was searched with a fragment ion mass tolerance of 0.060 Da
481 and a parent ion tolerance of 10.0 PPM. Deamidated of asparagine and glutamine,
482 oxidation of methionine, phospho of serine, threonine and tyrosine, GG of lysine, N-
483 ethylmaleimide of cysteine were specified in Mascot as variable modifications. Scaffold
484 (version Scaffold_4.8.9, Proteome Software Inc., Portland, OR) was used to validate
485 MS/MS based peptide and protein identifications. Peptide identifications were accepted
486 if they could be established at greater than 80.0% probability by the Peptide Prophet
487 algorithm[46] with Scaffold delta-mass correction. Protein identifications were accepted if
488 they could be established at greater than 99.0% probability and contained at least 2
489 identified peptides. Protein probabilities were assigned by the Protein Prophet
490 algorithm[47]. Proteins that contained similar peptides and could not be differentiated
491 based on MS/MS analysis alone were grouped to satisfy the principles of parsimony.
492 Proteins sharing significant peptide evidence were grouped into clusters.

493 **Liquid-Liquid Phase Separation (LLPS)**

494 LLPS of GFP-Clr4^{Full} and GFP-Clr4^{IDR} proteins were induced by diluting protein to 12
495 μM and 16 μM respectively in 20 mM Tris, pH 7.5, 30 mM NaCl, 0.5 mM MgAc, 1%
496 Glycerol and 15 mM Imidazole. To observe the effect of ubiquitin on GFP-Clr4^{IDR} LLPS,
497 0.9 μg/μl of human ubiquitin (R&D systems U-100H) or buffer only (10 mM Hepes, pH
498 7.6) were added to the GFP-Clr4^{IDR}. To observe the effect of 1,6-Hexanediol (Sigma

499 H11807) on GFP-Clr4^{IDR} LLPS, GFP-Clr4^{IDR} protein was diluted to 44.8 μM in 56 mM
500 Tris, pH 7.5, 84 mM NaCl, 1.4 mM MgAc, 2.8% Glycerol, 42 mM Imidazole and 3.6%
501 PEG8000 with or without 7.2% 1,6-Hexanediol. LLPS was imaged on Zeiss Axio Imager
502 M2 with differential interference contrast (DIC) and EGFP channels and processed
503 using Zeiss Zen software.

504 **FRAP experiments**

505 FRAP experiments were performed as previously described[48]. Briefly, GFP-Clr4^{IDR}
506 protein were diluted to 44.8 μM in 56 mM Tris, pH 7.5, 84 mM NaCl, 1.4 mM MgAc,
507 2.8% Glycerol, 42 mM Imidazole and 3.6% PEG8000 with or without 0.65 μg/μl
508 ubiquitin. FRAP experiments were carried out using Zeiss LSM710 Confocal Laser
509 Scanning Microscope with 63x objective. All Bleaching experiments were performed
510 with 488 nm argon laser at 100% intensity. Images before and after photobleaching
511 were taken at 5 s interval and analyzed using standard methods.

512 **Data availability**

513 Genome-wide datasets are deposited in the Gene Expression Omnibus (GEO) under
514 the accession number GSE156069. The token for private access is **ojipouckhladzeh.**

515

516 **Additional references for Materials and Methods**

517 4 Verdel, A. *et al.* RNAi-mediated targeting of heterochromatin by the RITS
518 complex. *Science* **303**, 672-676, doi:10.1126/science.1093686 (2004).

519 29 Kim, H. S. *et al.* Identification of a BET family bromodomain/casein kinase II/TAF-
520 containing complex as a regulator of mitotic condensin function. *Cell Rep* **6**, 892-
521 905, doi:10.1016/j.celrep.2014.01.029 (2014).
522 38 Bähler, J. *et al.* Heterologous modules for efficient and versatile PCR-based
523 gene targeting in Schizosaccharomyces pombe. *Yeast* **14**, 943-951,
524 doi:10.1002/(sici)1097-0061(199807)14:10<943::Aid-yea292>3.0.Co;2-y (1998).
525 39 Murray, J. M., Watson, A. T. & Carr, A. M. Transformation of
526 Schizosaccharomyces pombe: Lithium Acetate/ Dimethyl Sulfoxide Procedure.
527 *Cold Spring Harb Protoc* **2016**, pdb.prot090969, doi:10.1101/pdb.prot090969
528 (2016).
529 40 Langmead, B., Trapnell, C., Pop, M. & Salzberg, S. L. Ultrafast and memory-
530 efficient alignment of short DNA sequences to the human genome. *Genome Biol*
531 **10**, R25, doi:10.1186/gb-2009-10-3-r25 (2009).
532 41 Quinlan, A. R. & Hall, I. M. BEDTools: a flexible suite of utilities for comparing
533 genomic features. *Bioinformatics* **26**, 841-842, doi:10.1093/bioinformatics/btq033
534 (2010).
535 42 Winston, F. EMS and UV mutagenesis in yeast. *Curr Protoc Mol Biol* **Chapter**
536 **13**, Unit 13.13B, doi:10.1002/0471142727.mb1303bs82 (2008).
537 43 Roche, B., Arcangioli, B. & Martienssen, R. A. RNA interference is essential for
538 cellular quiescence. *Science* **354**, doi:10.1126/science.aah5651 (2016).
539 44 Langmead, B. & Salzberg, S. L. Fast gapped-read alignment with Bowtie 2. *Nat*
540 *Methods* **9**, 357-359, doi:10.1038/nmeth.1923 (2012).

541 45 Garrison, E. & Marth, G. Haplotype-based variant detection from short-read
542 sequencing. *arXiv e-prints*, arXiv:1207.3907 (2012).
543 <https://ui.adsabs.harvard.edu/abs/2012arXiv1207.3907G>.
544 46 Keller, A., Nesvizhskii, A. I., Kolker, E. & Aebersold, R. Empirical statistical model
545 to estimate the accuracy of peptide identifications made by MS/MS and database
546 search. *Anal Chem* **74**, 5383-5392, doi:10.1021/ac025747h (2002).
547 47 Nesvizhskii, A. I., Keller, A., Kolker, E. & Aebersold, R. A statistical model for
548 identifying proteins by tandem mass spectrometry. *Anal Chem* **75**, 4646-4658,
549 doi:10.1021/ac0341261 (2003).
550 48 Wang, H. *et al.* Rubisco condensate formation by CcmM in β-carboxysome
551 biogenesis. *Nature* **566**, 131-135, doi:10.1038/s41586-019-0880-5 (2019).
552

553 **Acknowledgement**

554 We thank all Martienssen lab members for valuable discussions and suggestions. This
555 work was supported by the Howard Hughes Medical Institute-Gordon and Betty Moore
556 Foundation (GMBF3033) and a grant from the National Institute of Health (GM076396)
557 (to R.A.M.).

558 **Author contributions**

559 H.S.K. performed experiments and bioinformatics. B.R. contributed sRNA-seq
560 experiments and bioinformatics. S.B. contributed to IP for ubiquitinated Clr4 and *in vitro*
561 protein purification. A.Y.C. contributed to EMS mutagenesis, C.H. contributed to LLPS

562 and LT and AV contributed to Rik1-TAP purification. H.S.K. and R.A.M. designed the
563 experiments and wrote the manuscript.

564 Competing interests

565 The authors declare no competing interests.

Supplementary Information Table 1. *S. pombe* strains used in this study.

Number	Name	Genotype	Reference
FY2002	WT	*h⁺ otrIR(SphI)::ade6 ImrIL(NcoI)::leul-32 ade6-DN/N ura4-DS/E leu1-32*	R. Allshire
HSK29	*ubc4-G48D* (*ubc4-1*)	FY2002_*ubc4-G48D-KanMX6*	This study
HSK335	*cul4-GFP* (*cul4-1*)	FY2002_*cul4-GFP-KanMX6*	This study
HSK351	*clr4Δ*	FY2002_*clr4Δ::KanMx6*	This study
HSK770	*dcr1Δ*	FY2002_*dcr1Δ::NatMx6*	This study
HSK790	*dcr1Δ ubc4-1*	FY2002_*dcr1Δ::NatMx6 ubc4-G48D-KanMX6*	This study
HSK606	*3xFlag-Clr4*	FY2002_*HphMX6-3xFlag-Clr4*	This study
HSK618	*3xFlag-Clr4 ubc4-1*	FY2002_*HphMX6-3xFlag-Clr4 ubc4-G48D-KanMX6*	This study
HSK1118	*3xFlag-Clr4-AllKtoR*	FY2002_*HphMX6-3xFlag-Clr4-AllKtoR*	This study
HSK971	*3xFlag-Clr4-2-8KtoR*	FY2002_*HphMX6-3xFlag-Clr4-2-8KtoR*	This study
HSK1121	*3xFlag-Clr4-2-4KtoR*	FY2002_*HphMX6-3xFlag-Clr4-2-4KtoR*	This study
HSK918	*3xFlag-Clr4 ubp3-OE*	FY2002_*HphMX6-3xFlag-Clr4 NatMX6-adh1p-ubp3*	This study
HSK1049	*3xFlag-Clr4-W31G*	FY2002_*HphMX6-3xFlag-Clr4-W31G*	This study
HSK1054	*3xFlag-Clr4-W31G ubc4-1*	FY2002_*HphMX6-3xFlag-Clr4-W31G ubc4-G48D-KanMX6*	This study
HSK679	*GFP-Swi6*	FY2002_*HphMX6-GFP-Swi6*	This study
HSK778	*GFP-Swi6 clr4Δ*	FY2002_*HphMX6-GFP-Swi6 clr4Δ::KanMX6*	This study
HSK700	*GFP-Swi6 ubc4-1*	FY2002_*HphMX6-GFP-Swi6 ubc4-G48D-KanMX6*	This study
HSK776	*GFP-Swi6 dcr1Δ*	FY2002_*HphMX6-GFP-Swi6 dcr1Δ::NatMX6*	This study
HSK808	*GFP-Swi6 dcr1Δ ubc4-1*	FY2002_*HphMX6-GFP-Swi6 dcr1Δ::NatMX6 ubc4-G48D-KanMX6*	This study
HSK518	*bdf2Δ*	FY2002_*bdf2Δ::KanMX6*	This study
HSK543	*ubc4-1 bdf2Δ*	FY2002_*ubc4-G48D-KanMX6 bdf2Δ::NatMX6*	This study
HSK545	*cul4-1 bdf2Δ*	FY2002_*cul4-GFP-KanMX6 bdf2Δ::NatMX6*	This study
HSK524	*Bdf2-3xFlag*	FY2002_ *Bdf2-3xFlag-HphMX6*	This study
HSK571	*Bdf2-3xFlag ubc4-1*	FY2002_ *Bdf2-3xFlag-HphMX6 ubc4-G48D-KanMX6*	This study
HSK573	*Bdf2-3xFlag cul4-1*	FY2002_ *Bdf2-3xFlag-HphMX6 cul4-GFP-KanMX6*	This study
HSK583	*Bdf2-3xFlag ddb1Δ*	FY2002_ *Bdf2-3xFlag-HphMX6 ddb1Δ::KanMX6*	This study
HSK575	*Bdf2-3xFlag clr3Δ*	FY2002_ *Bdf2-3xFlag-HphMX6 clr3Δ::KanMX6*	This study
HSK458	*cul4-1 ubc4-1*	FY2002_*cul4-GFP-KanMX6 ubc4-G48D-NatMX6*	This study
HSK608	*ubc4::mUBE2D2*	FY2002_*KanMX6-ubc4::mUBE2D2*	This study
HSK610	*ubc4::mUBE2D2-G48D*	FY2002_*KanMX6-ubc4::mUBE2D2-G48D*	This study
KFP26	*h⁻*	*h⁻ ura4-D18 leu1-32 ade6-M210 his3-D1*	Lab stock
SPG18	*h⁹⁰*	*h⁹⁰ ura4-D18 leul-32 ade6 -M216 his2*	Lab stock
DI304	*h⁹⁰ ubc4-G48D*	*h⁹⁰ leul-32 ubc4-G48D-KanMX6*	Irvine et al 2009
AY709	*h⁹⁰ubc4-G48D/S137T*	*h⁹⁰ leul-32 ubc4-G48D-KanMX6 ubc4-S137T* (EMS mutagenesis)	This study
HSK33	*raf1Δ*	FY2002_*raf1Δ::KanMx6*	This study
HSK307	*raf2Δ*	FY2002_*raf2Δ::KanMx6*	This study
HSK355	*rik1Δ*	FY2002_*rik1Δ::KanMx6*	This study
HSK351	*clr3Δ*	FY2002_*clr3Δ::KanMx6*	This study
HSK644	*ubc4-3xHA*	FY2002_*ubc4-3xHA-KanMX6*	This study
HSK646	*cul4Δ*	FY2002_*cul4Δ::NatMx6*	This study
HSK716	*GFP-Swi6 ubc4-3xHA*	FY2002_*HphMX6-GFP-Swi6 ubc4-3xHA-KanMX6*	This study
HSK717	*GFP-Swi6 cul4Δ*	FY2002_*HphMX6-GFP-Swi6 cul4Δ::NatMX6*	This study
HSK642	*ubc4-GFP*	FY2002_*ubc4-GFP-KanMX6*	This study
HSK393	*3xFlag-Rik1*	FY2002_*HphMX6-3xFlag-Rik1*	This study
HSK389	*3xFlag-Raf1*	FY2002_*HphMX6-3xFlag-Raf1*	This study
HSK274	*Raf2-3xFlag*	FY2002_*Raf2-3xFlag-HphMX6*	This study
HSK620	*3xFlag-Clr4 cul4-1*	FY2002_*HphMX6-3xFlag-Clr4 cul4-GFP-KanMX6*	This study
HSK920	*3xFlag-Clr4 rik1Δ*	FY2002_*HphMX6-3xFlag-Clr4 rik1Δ::NatMx6*	This study
HSK921	*3xFlag-Clr4 raf1Δ*	FY2002_*HphMX6-3xFlag-Clr4 raf1Δ::NatMx6*	This study

Number	Name	Genotype	Reference
HSK922	*3xFlag-Clr4 raf2Δ*	FY2002_*HphMX6-3xFlag-Clr4 raf2Δ::NatMx6*	This study
HSK1125	*3xFlag-Clr4-1-6KtoR*	FY2002_*HphMX6-3xFlag-Clr4-1-6KtoR*	This study
HSK1127	*3xFlag-Clr4-3-6KtoR*	FY2002_*HphMX6-3xFlag-Clr4-3-6KtoR*	This study
HSK1129	*3xFlag-Clr4-4-6KtoR*	FY2002_*HphMX6-3xFlag-Clr4-4-6KtoR*	This study
HSK1131	*3xFlag-Clr4-5-5KtoR*	FY2002_*HphMX6-3xFlag-Clr4-5-5KtoR*	This study
HSK1132	*3xFlag-Clr4-6-5KtoR*	FY2002_*HphMX6-3xFlag-Clr4-6-5KtoR*	This study
HSK1140	*3xFlag-Clr4-K87R*	FY2002_*HphMX6-3xFlag-Clr4-K87R*	This study
HSK1142	*3xFlag-Clr4-K94R*	FY2002_*HphMX6-3xFlag-Clr4-K94R*	This study
HSK1144	*3xFlag-Clr4-K109R*	FY2002_*HphMX6-3xFlag-Clr4-K109R*	This study
HSK1146	*3xFlag-Clr4-K110R*	FY2002_*HphMX6-3xFlag-Clr4-K110R*	This study
HSK1148	*3xFlag-Clr4-K113R*	FY2002_*HphMX6-3xFlag-Clr4-K113R*	This study
HSK1150	*3xFlag-Clr4-K114R*	FY2002_*HphMX6-3xFlag-Clr4-K114R*	This study
HSK1152	*3xFlag-Clr4-K122R*	FY2002_*HphMX6-3xFlag-Clr4-K122R*	This study
HSK1154	*3xFlag-Clr4-K127R*	FY2002_*HphMX6-3xFlag-Clr4-K127R*	This study
HSK1013	*3xFlag-clr4-K109/110/113/114R*	FY2002_*HphMX6-3xFlag-Clr4-K109/110/113/114R-KanMX6*	This study
HSK999	*3xFlag-Clr4-K87/94/109/110/113/114R*	FY2002_*HphMX6-3xFlag-Clr4-K87/94/109/110/113/114R-KanMX6*	This study
HSK1000	*3xFlag-Clr4-K109/110/113/114/122/127R*	FY2002_*HphMX6-3xFlag-Clr4-K109/110/113/114/122/127R-KanMX6*	This study
HSK1015	*3xFlag-Clr4-K110/113/114R*	FY2002_*HphMX6-3xFlag-Clr4-110/113/114R-KanMX6*	This study
HSK1017	*3xFlag-Clr4-K109/113/114R*	FY2002_*HphMX6-3xFlag-Clr4-109/113/114R-KanMX6*	This study
HSK1019	*3xFlag-Clr4-K109/110/114R*	FY2002_*HphMX6-3xFlag-Clr4-109/110/114R-KanMX6*	This study
HSK1021	*3xFlag-Clr4-K109/110/113R*	FY2002_*HphMX6-3xFlag-Clr4-109/110/113R-KanMX6*	This study
HSK1082	*3xFlag-Clr4-K109/110R*	FY2002_*HphMX6-3xFlag-Clr4-109/110R-KanMX6*	This study
HSK1062	*3xFlag-Clr4-K109/113R*	FY2002_*HphMX6-3xFlag-Clr4-109/113R-KanMX6*	This study
HSK1064	*3xFlag-Clr4-K109/114R*	FY2002_*HphMX6-3xFlag-Clr4-109/114R-KanMX6*	This study
HSK1086	*3xFlag-Clr4-K110/113R*	FY2002_*HphMX6-3xFlag-Clr4-110/113R-KanMX6*	This study
HSK1065	*3xFlag-Clr4-K110/114R*	FY2002_*HphMX6-3xFlag-Clr4-110/114R-KanMX6*	This study
HSK1084	*3xFlag-Clr4-K113/114R*	FY2002_*HphMX6-3xFlag-Clr4-113/114R-KanMX6*	This study
HSK919	*3xFlag-Clr4 ubp3Δ*	FY2002_*HphMX6-3xFlag-Clr4 ubp3Δ::NatMx6*	This study
HSK395	*ubp3-OE***	FY2002_*HphMX6-adh1p-ubp3* (*ubp3* overexpression)	This study
HSK401	*ubp8-OE***	FY2002_*HphMX6-adh1p-ubp8* (*ubp8* overexpression)	This study

Supplementary Information Table 2. Oligonucleotides used in this study.

Name	Description	Purpose	Sequence
p30-qPCR-F	*dg*	ChIP-qPCR, RT-qPCR	CCATATCAATTTCCCATGTTCC
p30-qPCR-R	*dg*	ChIP-qPCR, RT-qPCR	CATCAAGCGAGTCGAGATGA
p33-qPCR-F	*dh*	ChIP-qPCR, RT-qPCR	TATCCTGCGTCTCGGTATCC
p33-qPCR-R	*dh*	ChIP-qPCR, RT-qPCR	CTGTTCGTGAATGCTGAGAAAG
act1-qPCR-F	*act1*	ChIP-qPCR, RT-qPCR	TGCACCTGCCTTTTATGTTG
act1-qPCR-F	*act1*	ChIP-qPCR, RT-qPCR	TGGGAACAGTGTGGGTAACA
ade6-qPCR-F	*ade6*	ChIP-qPCR	TTCCTACTGCCATCAAAGCA
ade6-qPCR-R	*ade6*	ChIP-qPCR	GCACGCTGTTGAATTGAGAA
ura4-qPCR-F	*ura4*	ChIP-qPCR	TACCTTTGGGACGTGGTCTC
ura4-qPCR-R	*ura4*	ChIP-qPCR	CCCGTCTCCTTTAACATCCA
irc3-R-qPCR-F	*irc-3R*	ChIP-qPCR	GGCAACCTTTCAAGTTCTCG
irc3-R-qPCR-R	*irc-3R*	ChIP-qPCR	ATTCTTCCCATCTGCGTTTG
tlh1-R-qPCR-F	*tlh1*	ChIP-qPCR	GTTCTCCATGCTCCACTGGT
tlh1-R-qPCR-R	*tlh1*	ChIP-qPCR	CCAACAGTGGTCTTCGGTTT
ubp3-qPCR-F	*ubp3*	RT-qPCR	GCCAAATTTTTGGTGGTCAG
ubp3-qPCR-R	*ubp3*	RT-qPCR	TGAATGTCGAGTTGCAGAGG
Clr4(His)-NdeI-F	6xHis-Clr4	Plasmid construction	CCGCGCGGCAGCCATATGTCGCCTAAACAAGAGGAGTATG
Clr4(His)-NdeI-R	6xHis-Clr4	Plasmid construction	CGGATCCTCGAGCATATGTTAACCGAAAAGCCAGCCACGACAA
Clr4-BamHI-F	6xHis-GFP-Clr4	Plasmid construction	CGGGTACCATGGATCCGATGTCGCCTAAACAAGAGGAGTATG
Clr4-XhoI-R	6xHis-GFP-Clr4	Plasmid construction	GGTGGTGGTGCTCGAGTTAACCGAAAAGCCAGCCACGACAA
Clr4-IDR-BamHI-F	6xHis-GFP-IDR	Plasmid construction	CGGGTACCATGGATCCGTCTGCCGTTTTAGCAGAATGGAAAA
Clr4-IDR-XhoI-R	6xHis-GFP-IDR	Plasmid construction	GGTGGTGGTGCTCGAGCTATTCGGGTCCTTCAATTTCCCGC

Supplementary Information Table 3. Plasmids used in this study.

Name	Description	Application
pET-14b-Clr4	6xHis-Clr4	Recombinant 6xHis-Clr4 protein purification from *E. coli*
pHis-parellel-GFP-Clr4^{Full}	6xHis-GFP-Clr4^{Full}	Recombinant 6xHis-GFP-Clr4^{Full} protein purification from *E. coli*
pHis-parellel-GFP-Clr4^{IDR}	6xHis-GFP-Clr4^{IDR}	Recombinant 6xHis-GFP-Clr4^{IDR} protein purification from *E. coli*

Figure 1

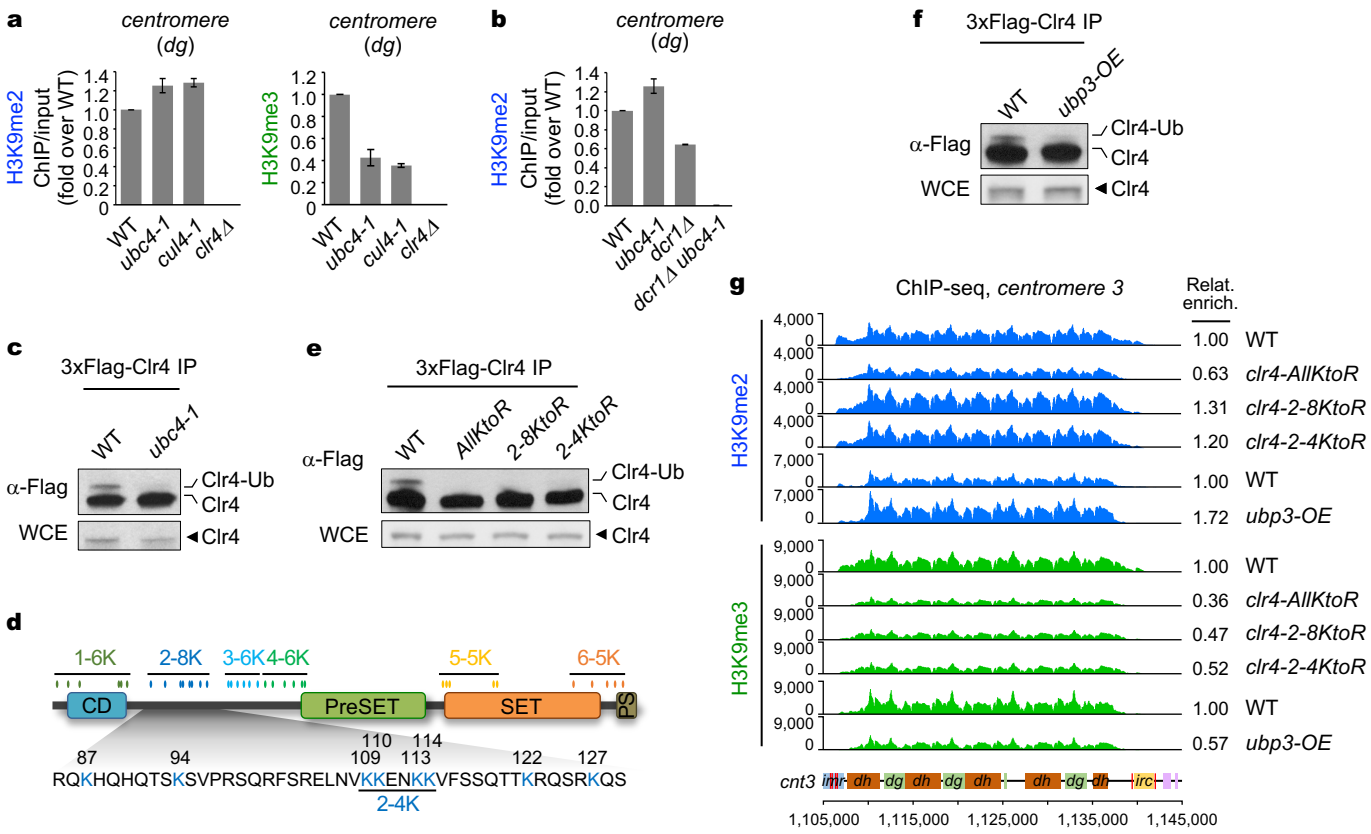

Figure 1. Mono-ubiquitination of Clr4 by Ubc4-CLRC is required for H3K9 trimethylation.

a, ChIP-qPCR assays showing enrichment of H3K9me2 (left) and H3K9me3 (right) at centromeric *dg* locus in the indicated strains. *clr4* deletion mutant (*clr4Δ*) shows complete loss of H3K9me2 and H3K9me3. Error bars, standard deviation (S.D., 3 biological replicates).

b, ChIP-qPCR assays showing enrichment of H3K9me2 at centromeric *dg* locus in the indicated strains. *dcr1Δ ubc4-1* double mutant shows complete abolishment of H3K9me2. Error bars, S.D. (3 biological replicates).

c, Western blot (WB) analyses of immunoprecipitated 3xFlag-Clr4 (3xFlag IP) from WT and *ubc4-1* mutant cells treated with proteasome inhibitor MG-132 (100μM) for 4 h before harvest. Bottom, WB analysis of 3xFlag-Clr4 from whole cell extract (WCE).

d, Schematic diagram of domain structure of Clr4 protein and the position of lysine residues. CD: chromodomain, PS: PostSET. Ovals show the position of all 36 lysines of Clr4, which are subgrouped to 6 groups. Second group (2-8K) is highlighted and amino acid sequences are shown. 2-4K region covers K109-K114.

e, WB analyses same as **c**, but showing WT, all-lysine mutant (*AllKtoR*), second block mutant (*2-8KtoR*) and mutant of 4 lysines (K109, K110, K113 and K114) of second block (*2-4KtoR*).

f, Western blot (WB) analysis of immunoprecipitated 3xFlag-Clr4 from WT and *ubp3*-overexpression *(ubp3-OE)* strains.

g, ChIP-seq reads of H3K9me2 and H3K9me3 mapped to chromosome 3 centromere right arm in the indicated strains. Relat. enrich., relative enrichemnt. Total count of ChIP-seq reads from different strains were divided by the total count of WT to show relative enrichment. Bottom, schematic diagram of chromosome 3 centromere right arm showing innermost repeat (*imr*), outermost repeats (*dg*, *dh*) and boundary region (*irc*) between heterochromatin and euchromatin. Vertical red lines and pink boxes represent tRNA and euchromatic genes respectively.

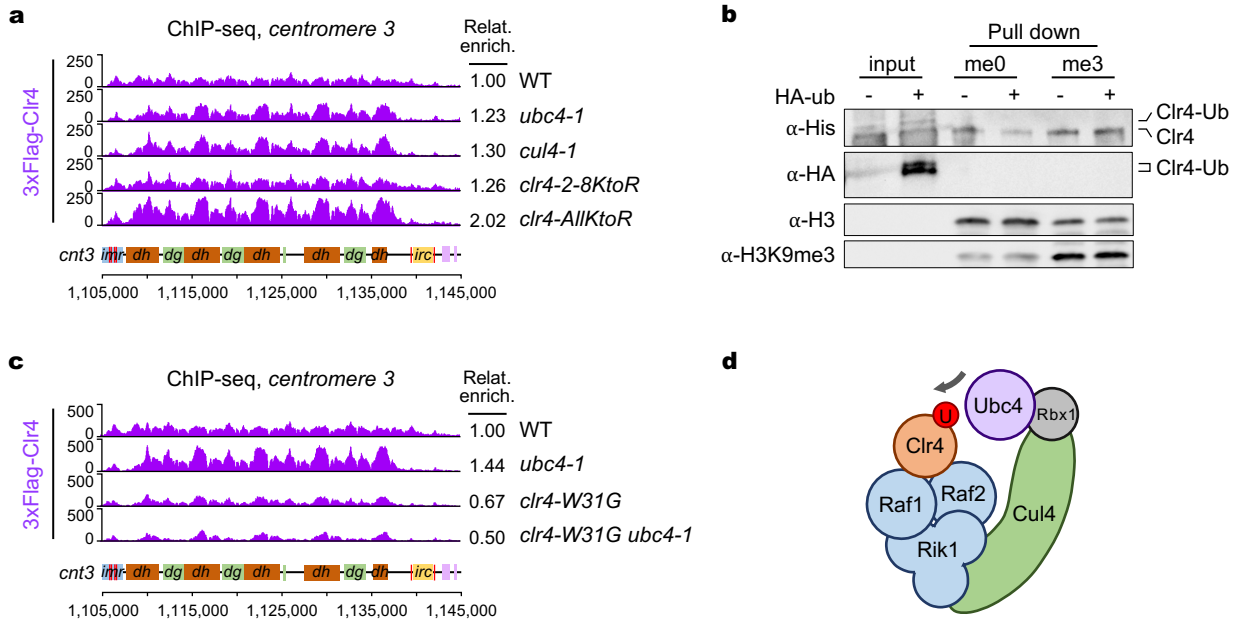

Figure 2. **Clr4 mono-ubiquitination induces its dissociation from chromatin.**

a, ChIP-seq reads of 3xFlag-Clr4 mapped to chromosome 3 centromere (*cnt3*) right arm in indicated strains. Relat. enrich., relative enrichemnt. Bottom, schematic diagram of chromosome 3 centromere (*cnt3*) right arm.

b, *In vitro* protein binding assay of *in vitro* ubiquitinated Clr4 protein with nucleosomes. His-Clr4 purified from *E. coli* cells was ubiquitinated with human E1, E3 (UBE2D3) and HA-ubiquitin and incubated with nucleosomes with unmodified histone H3 (me0) or H3K9me3 histone (me3) anchored to streptavidin beads. Input and precipitated proteins were analyzed by Western blot (WB) using antibodies as shown.

c, ChIP-seq reads of 3xFlag-Clr4 mapped to chromosome 3 centromere (*cnt3*) right arm in indicated strains. Relat. enrich., relative enrichment. Bottom, schematic diagram of chromosome 3 centromere (*cnt3*) right arm.

d, Schematic diagram showing the presumptive subunit arrangement in the complex of Ubc4-CLRC and its substrate Clr4. Red circle (U), ubiquitin. The arrow shows the mono-ubiquitination activity of Ubc4-CLRC toward Clr4.

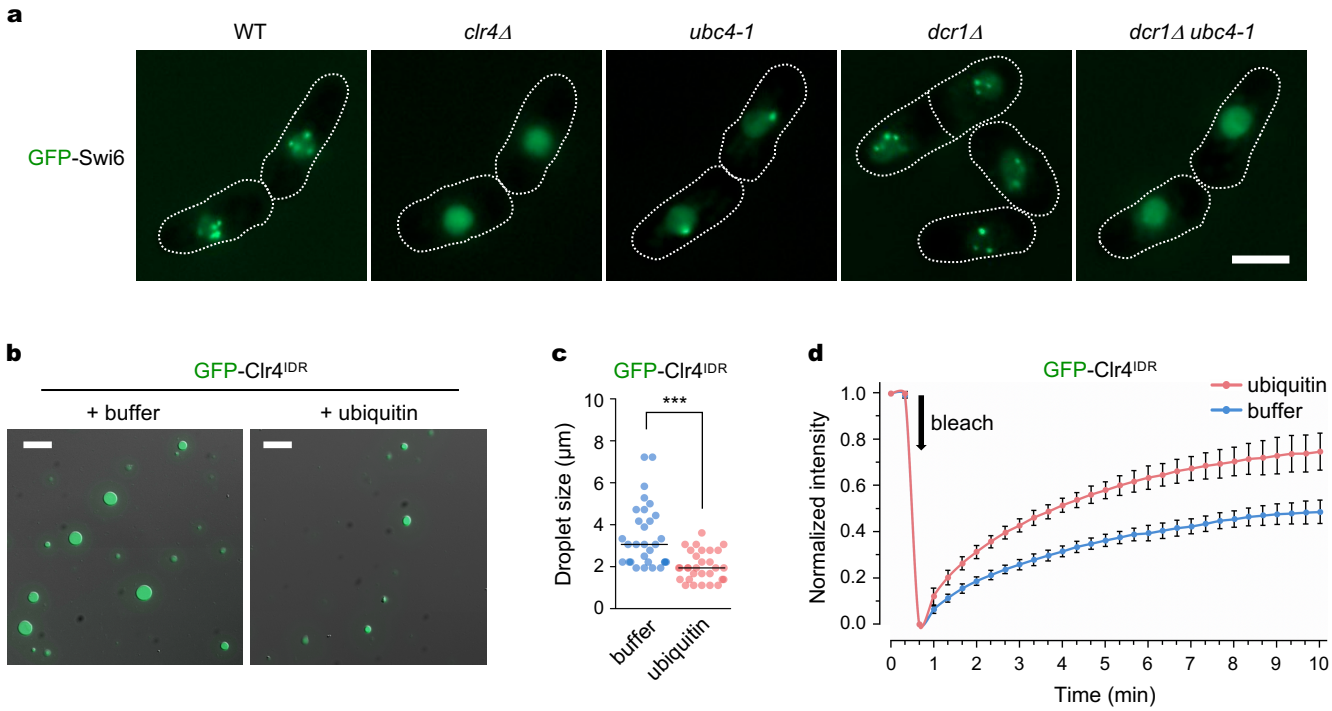

Figure 3. Ubiquitin reduces GFP-Clr4^{IDR} LLPS activity.

a. Live cell imaging showing GFP-Swi6 heterochromatic foci in indicated strains. In WT 4 foci represent three telomeres and the centromeric chromocenter, which disappears in *dcr1Δ*. Only the chromocenter focus is retained in *ubc4-1* which loses H3K9me from telomeres. The foci are completely abolished in *clr4Δ* and *dcr1Δ ubc4-1* mutants. Scale bar, 2.5μm. Dashed lines show the outline of each *S. pombe* cells.

b, Reduced size of LLPS of GFP-Clr4^{IDR} (amino acid 51-220) by addition of ubiquitin. Buffer or ubiquitin was added to GFP-Clr4^{IDR} protein and the formation of LLPS was monitored. Scale bar, 10μm.

c, Reduced size of LLPS of GFP-Clr4^{IDR} by addition of ubiquitin (**b**). Top 30 LLPS droplets are measured and size distribution is shown. Black bar, average. ****P* value=1.1X10^{-5}.

d, FRAP of GFP-Clr4^{IDR} by addition of ubiquitin before and after bleaching. The change of fluorescence was analyzed and indicated in mean and S.D. (n=7 and n=9 for Buffer and Ubiquitin, respectively). Arrow shows the time of bleaching (~40s).

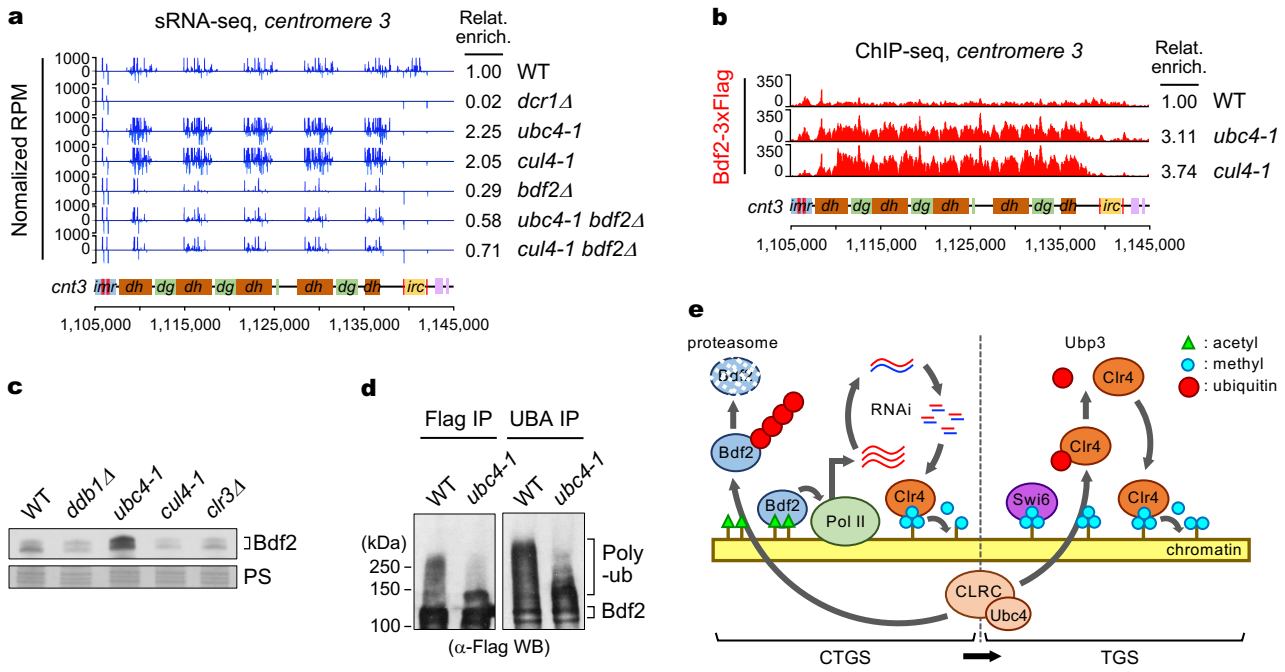

Figure 4. **Ubc4-CLRC poly-ubiquitinates Bdf2 and regulates sRNA production.**

a, sRNA-seq reads mapped to chromosome 3 centromere right arm. The increased sRNA production in *ubc4-1* and *cul4-1* mutants is suppressed by the deletion mutation of *bdf2*. sRNA at boundary region (*irc*) were abolished in all mutants. Remaining sRNA peaks in *dcr1Δ* are tRNA-related products. Relat. enrich., relative enrichment of sRNA without tRNA. Bottom, schematic diagram of chromosome 3 centromere right arm.

b, ChIP-seq reads of Bdf2-3xFlag mapped to chromosome 3 centromere (*cnt3*) right arm in indicated strains. Relat. enrich., relative enrichment. Bottom, schematic diagram of chromosome 3 centromere right arm.

c, Western blot (WB) analyses for Bdf2-3xFlag in indicated strains. Ponceau S staining of membrane is shown for equal loading of protein for WB.

d, Western blot (WB) analyses of immunoprecipitated Bdf2-3xFlag (Flag IP) from WT and *ubc4-1* mutant cells treated with proteasome inhibitor MG-132 (100μM) for 4 h before harvest (left). Bdf2-3xFlag enrichment by ubiquitination affinity beads (UAB IP) are shown on right.

e, Model for the function of Ubc4-CLRC-mediated Clr4 mono-ubiquitination and Bdf2 poly-ubiquitination. Left, Bdf2 recruits RNA Pol II complex to produce centromeric ncRNAs, which are converted to sRNAs by the sequencial action of RNAi machineries and these sRNAs reinforce the Clr4 activity for H3K9me2. Ubc4-CLRC poly-ubiquitinates Bdf2 for its degradation and reduces recruitment of RNA Pol II. Right, Clr4 converts H3K9me2 to H3K9me3 but because of its strong binding affinity to H3K9me3, it remains to bind nucleosome with H3K9me3. Clr4 mono-ubiquitination by Ubc4-CLRC dissociates Clr4 from chromatin and Ubp3 removes the mono-ubiquitin from Clr4. Unmodified Clr4 binds other nucleosomes with H3K9me3 and converts RNAi-independent H3K9me1 or -2 nucleosomes nearby to H3K9me3. Both reduction of sRNA and conversion of H3K9me2 to H3K9me3 promote the transition from CTGS to TGS.

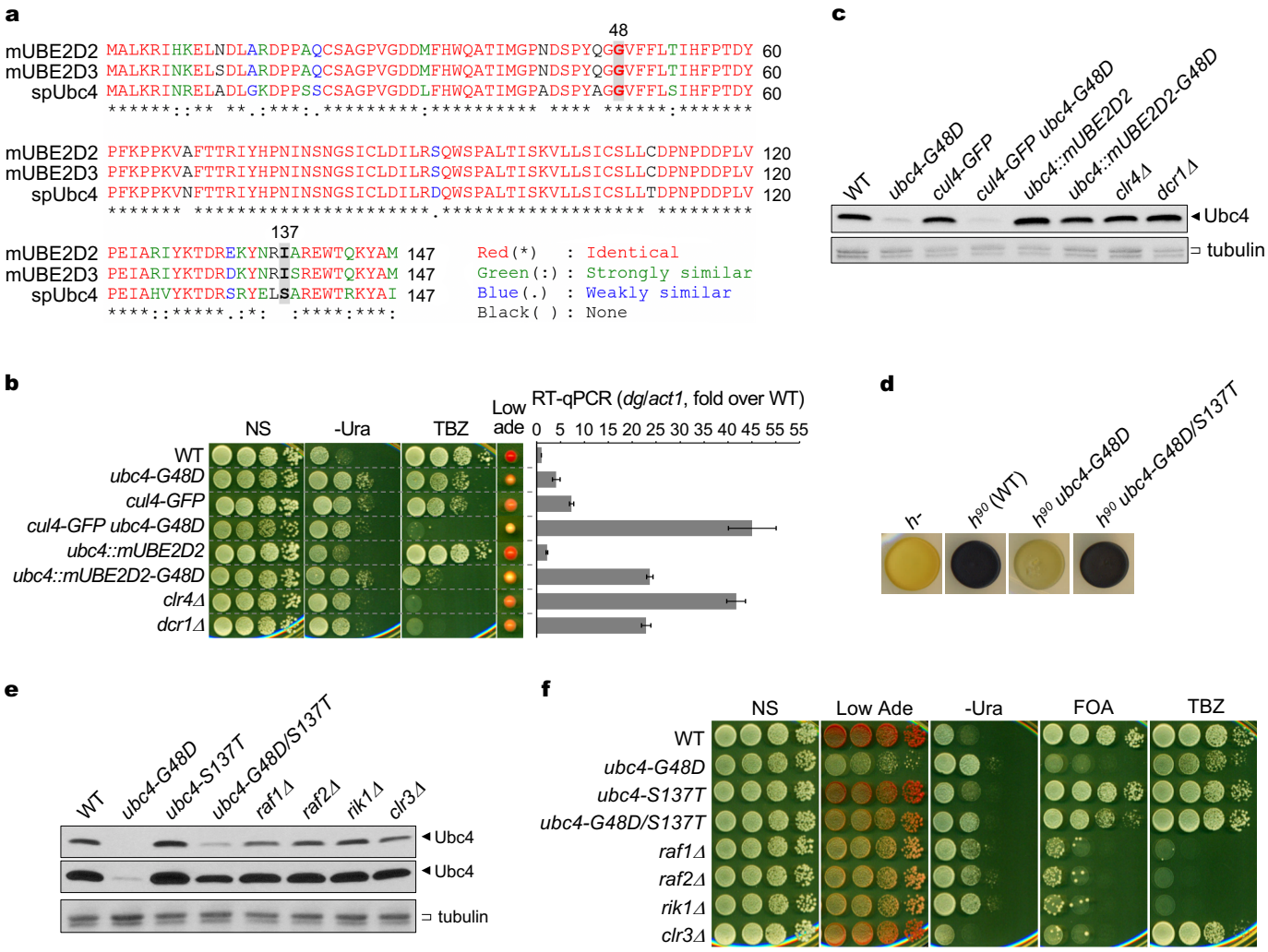

Extended Data Figure 1. Analysis of *ubc4* mutants and its protein stability.

a, Ubc4 shows strong amino acid sequence identity and similarity with its mouse homologues, mUBE2D2 and mUBE2D3. Glycine 48 of Ubc4 is conserved in mouse homologues but Serine 137 is not. Multiple sequence alignment of Ubc4 and its homologues was generated using Clustal Omega.

b, *ubc4-G48D* (*ubc4-1*) and *cul4-GFP* (*cul4-1*) mutants decrease heterochromatin silencing. Swapping *S. pombe ubc4* gene with mouse UBE2D2 gene complements essential function of Ubc4 and *mUBE2D2-G48D* also shows silencing defect. Left, silencing assay of *imr1L::ura4*$^+$ and *otr1R::ade6*$^+$ on no Uracil (-Ura) and low-adenine (Low ade) media to assess *ura4*$^+$ and *ade6*$^+$ expression and TBZ-sensitivity assay on 15μg/ml microtubule-destabilizing agent, thiabendazole (TBZ) in the indicated strains. NS, non-selective medium. Right, RT-qPCR analysis for centromeric *dg* transcription (normalized to *act1*). Error bars, S.D. (3 biological replicates).

c, Ubc4 protein is greatly reduced in *ubc4-G48D* mutant. For Western blot analysis of Ubc4 protein in the indicated strains, antibody for mUBE2D3 was used to detect Ubc4. Tubulin was used as loading control.

d, Mating-type switching defect in *ubc4-G48D* mutant was suppressed by the secondary mutation, *S137T*. Non-switchable h^- and WT and *ubc4-G48D* mutants in switchable strain (h^{90}) were plated and incubated on sporulation medium and spores were stained with iodine vapors. The enrichment of starch in spore enables staining with iodine and dark staining indicates the strain is switch competent and can make spores but light staining indicates the strain is switching defective and cannot make spores efficiently. *ubc4-S137T* mutation which was identified by EMS mutagenesis of *ubc4-G48D*, iodine staining and whole genome sequencing suppresses the mating switching defect of *ubc4-G48D* mutant (ubc4-*G48D/S137T*).

e, *ubc4-S137T* mutation restores decreased protein level of *ubc4-G48D* mutant. Western blot analysis of Ubc4 protein and tubulin as control. Middle panel shows the longer exposure of upper panel for Ubc4 protein.

f, *ubc4-S137T* mutation suppresses the silencing defect of *ubc4-G48D* mutant. Silencing assay is same with **b,** but FOA containing (FOA) media, which kills *ura4*$^+$ expressing cells, was also used to assess *ura4*$^+$ expression.

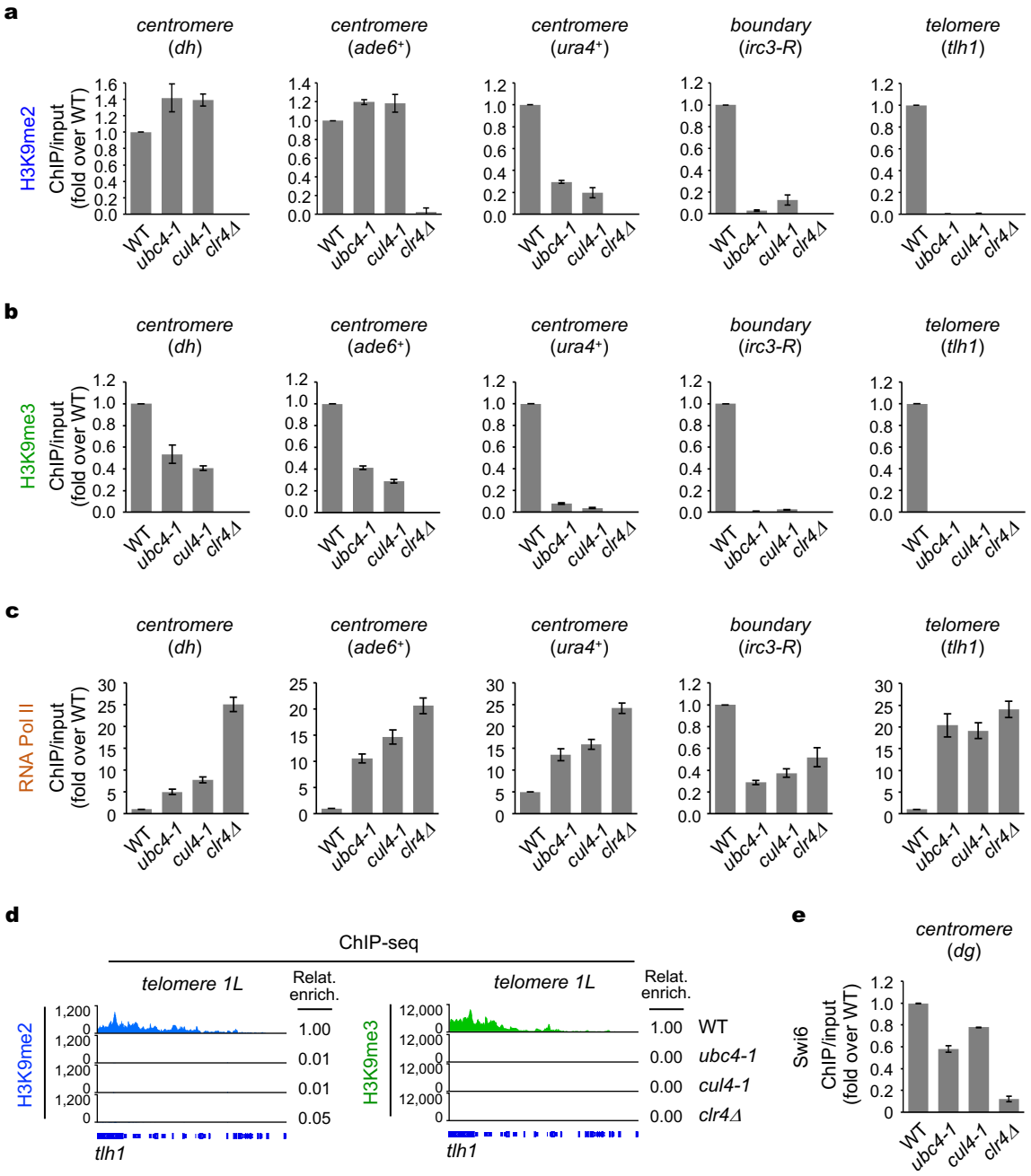

Extended Data Figure 2. Ubc4 and Cul4 regulate H3K9me status.

a-c, ChIP-qPCR assays showing enrichment of H3K9me2 (**a**), H3K9me3 (**b**) and RNA Pol II (Rpb1, **c**) at centromeric *dh*, *ade6*$^+$ and *ura4*$^+$ reporter genes at centromere, boundary region between heterochromatin and euchromatin of centromere 3 (*irc3-R*) and telomeric *tlh1* locus. Error bars, S.D. (3 biological replicates).

d, ChIP-seq reads of H3K9me2 (left) and H3K9me3 (right) mapped to telomere 1 left region. Relat. enrich., relative enrichment. Bottom, schematic diagrams of *tlh1* gene locus.

e, ChIP-qPCR assays showing slightly decreased enrichment of HP1 protein, Swi6 at centromeric *dg* locus in *ubc4-1* and *cul4-1* strains. Error bars, S.D. (2 biological replicates).

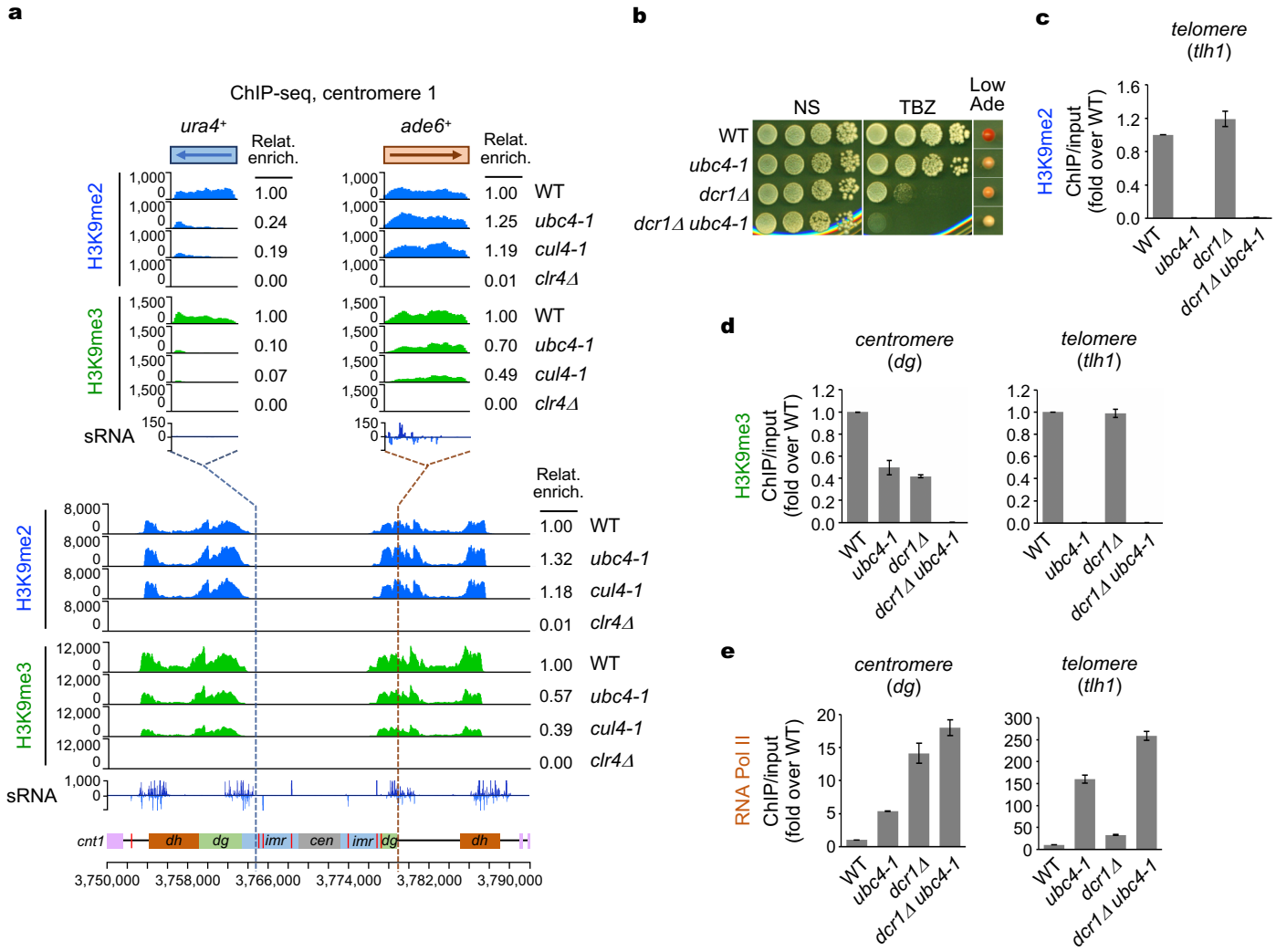

Extended Data Figure 3. Ubc4 and Cul4 regulate H3K9 methylation through RNAi

a, ChIP-seq reads of H3K9me2 and H3K9me3 mapped to chromosome 1 centromere (*cnt1*) in the indicated strains. Dashed lines indicates the loci where reporter genes, *ura4*$^+$ and *ade6*$^+$ are inserted at centromere 1. The change of H3K9me2 and H3K9me3 on *ura4*$^+$ and *ade6*$^+$ reporter genes are shown (top). Arrow in the box shows the direction of gene. sRNA-seq reads of WT are also shown. Relat. enrich., relative enrichment. Bottom, schematic diagram of chromosome 1 centromere (*cnt1*) showing innermost repeat (*imr*), outermost repeats (*dg*, *dh*) and centromere core (*cen*). Vertical red lines and pink boxes represent tRNA and euchromatic genes respectively.

b, TBZ-sensitivity assay on media containing 15μg/ml thiabendazole (TBZ) and silencing assay of *otr1R::ade6*$^+$ on low-adenine (Low ade) media in the indicated strains.

c, ChIP-qPCR assays showing enrichment of H3K9me2 at telomeric *tlh1* loci in the indicated strains. Error bars, S.D. (2 biological replicates).

d, ChIP-qPCR assays showing enrichment of H3K9me3 at centromeric *dg* and telomeric *tlh1* loci in the indicated strains. Error bars, S.D. (2 biological replicates).

e, ChIP-qPCR assays showing enrichment of RNA Pol II (Rpb1) at centromeric *dg* (left) and telomeric *tlh1* (right) loci in the indicated strains. Error bars, S.D. (2 biological replicates).

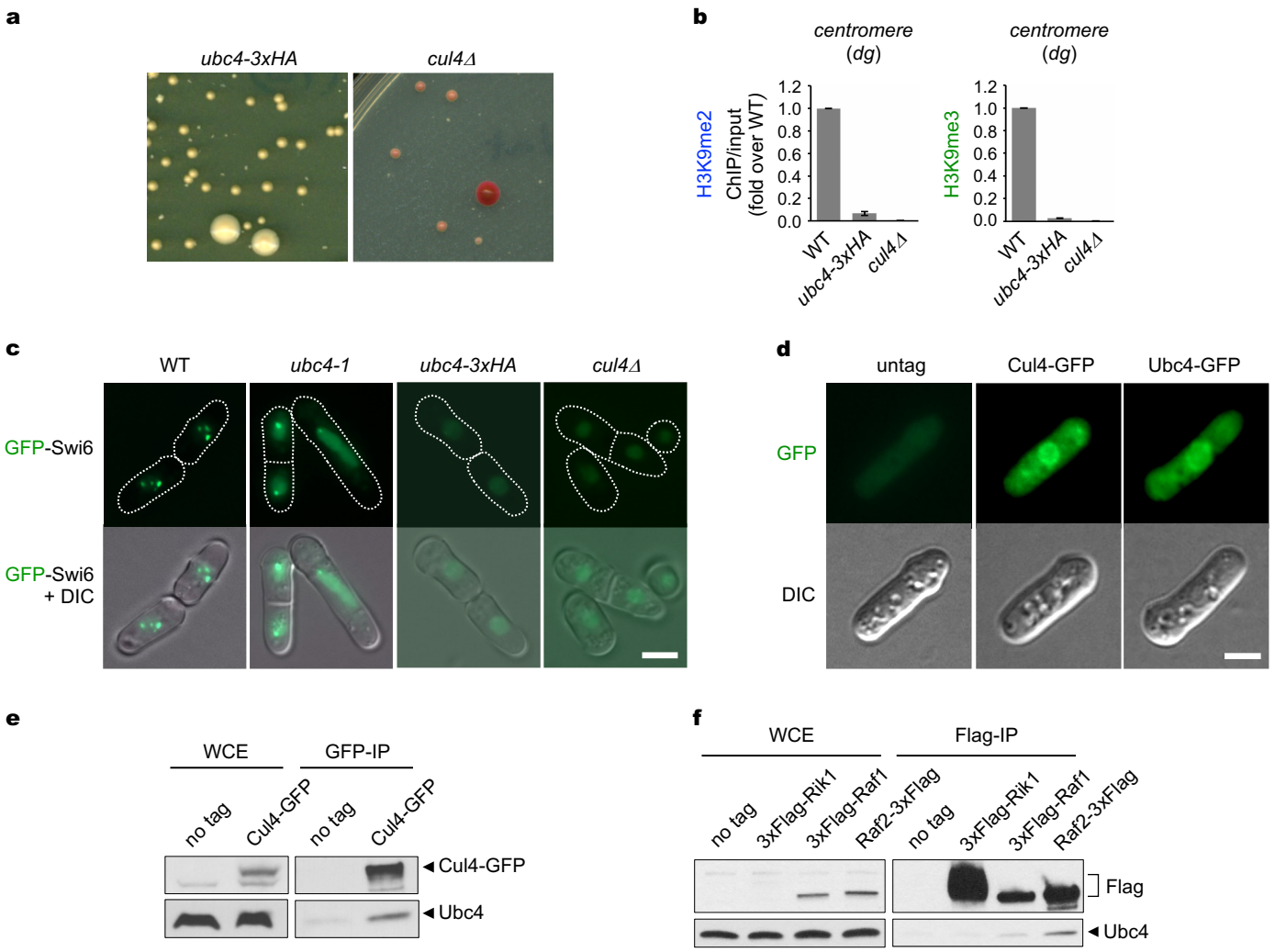

Extended Data Figure 4. Ubc4 and Cul4 localize to nuclear periphery and Ubc4 forms complex with CLRC.

a, *ubc4* mutant with triple HA tag at carboxyl-terminus (*ubc4-3xHA*) and *cul4* deletion mutant (*cul4Δ*) are viable but show severe growth defect. Big cells in each picture show WT cells. *ubc4-3xHA* cells were grown on YES media and *cul4Δ* cells were grown on low-adenine media.

b, ChIP-qPCR assays showing enrichment of H3K9me2 and H3K9me3 at centromeric *dg* locus in the indicated strains. Error bars, S.D. (2 biological replicates).

c. Live cell imaging showing the localization of GFP-Swi6 in indicated strains. The localization of GFP-Swi6 is completely abolished in *ubc4-3xHA* and *cul4Δ* mutants, which is consistent with H3K9me2 and H3K9me3 ChIP-qPCR results (**b**). Scale bar, 2.5μm.

d, Live cell imaging showing that Cul4-GFP and Ubc4-GFP localize to nuclear periphery. The strain without GFP tag (untag) was used as negative control. Scale bar, 2.5μm.

e, Co-immunoprecipitation (Co-IP) of Cul4-GFP with Ubc4. Whole-cell extracts (WCE) were immunoprecipitated with GFP antibody and Western blot analyses were carried out with GFP and mUBE2D3 antibodies.

f, Co-immunoprecipitation (Co-IP) of 3xFlag-Rik1, 3xFlag-Raf1 and Raf2-3xFlag with Ubc4. Whole-cell extracts (WCE) were immunoprecipitated with Flag antibody and Western blot analyses were carried out with Flag and mUBE2D3 antibodies.

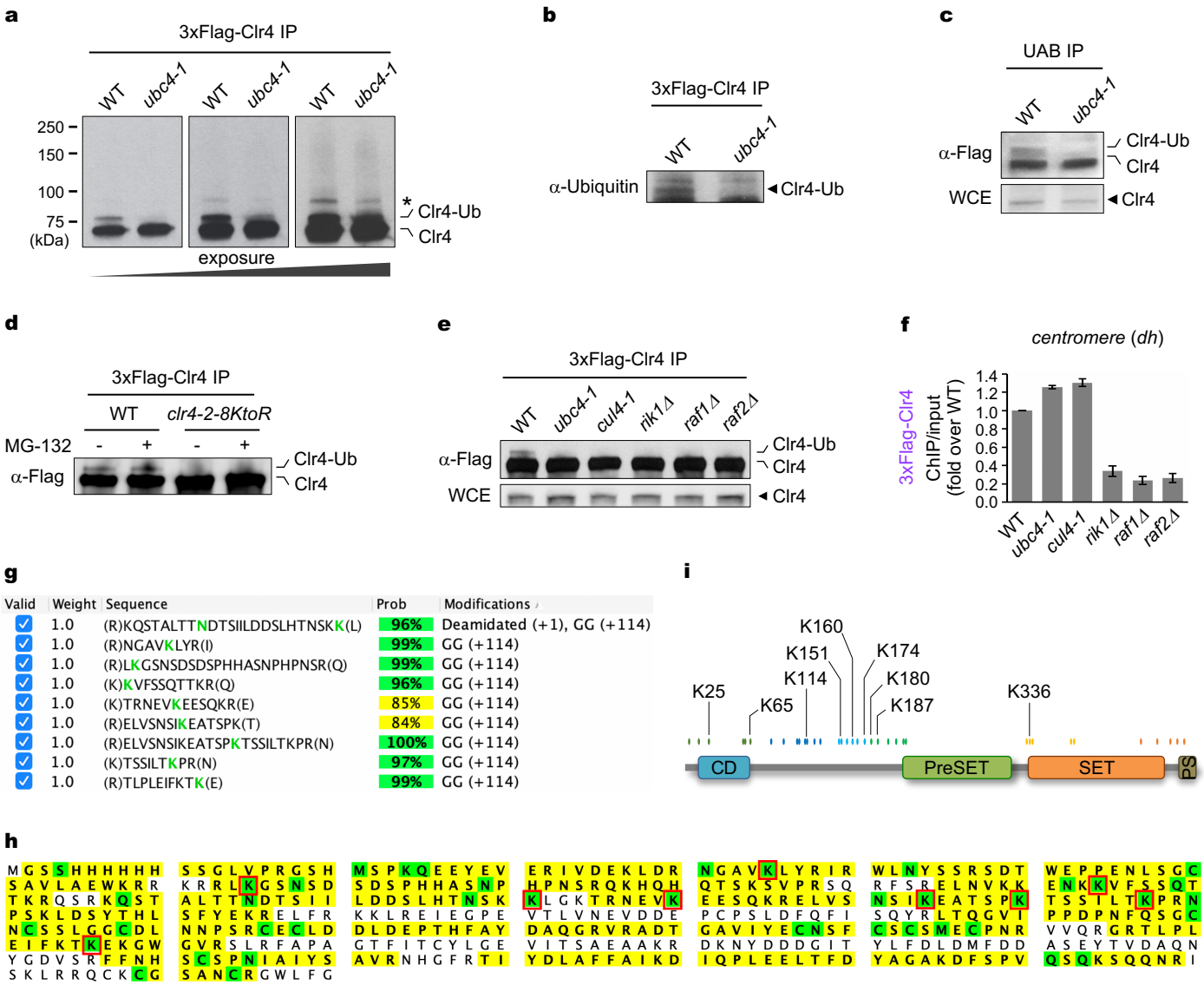

Extended Data Figure 5. Characterization of ubiquitination sites of Clr4 by Mass Spectrometry analysis.

a, same as Fig. 1c**,** but shows extended exposure of WB analysis for immunoprecipitated 3xFlag-Clr4 from WT and *ubc4-1* mutant cells. Asterisk indicates possible di- or multi-ubiquitin chain which is also largely dependent on Ubc4.

b, WB analysis for 3xFlag-Clr4 enriched by α-Flag affinity beads and WB analysis using ubiquitin antibody.

c, WB analyses same as Fig. 1c, but showing 3xFlag-Clr4 enrichment by ubiquitination affinity beads (UAB IP).

d, Proteasome pathway-independent Clr4 ubiquitination. Western blot (WB) analysis of immunoprecipitated 3xFlag-Clr4 from wild type (WT) and second block mutant (*2-8KtoR*) with or without treatment of proteasome inhibitor MG-132 for 4h before harvest.

e, WB analyses same as Fig. 1c, but showing also CLRC mutants like *cul4-1*, *rik1Δ*, *raf1Δ* and *raf2Δ*.

f, ChIP-qPCR assay showing enrichment of 3xFlag-Clr4 at centromeric *dh* locus in the indicated strains. Error bars, S.D. (2 biological replicates).

g, 6xHis-Clr4 purified from *E. coli* cells were *in vitro* ubiquitinated with human E1, E3 (UBE2D3) and ubiquitin and analyzed by Mass Spectrometry. The peptides with possible ubiquitination sites were shown. Di-glycine-Lysine (GG) remnants after trypsin digestion indicate possible ubiquitination sites. Prob., probability. Mass Spectrometry results were analyzed using Scaffold program.

h, Amino acid sequence of 6xHis-Clr4 protein. Sequence coverage by Mass Spectrometry analysis is highlighted in yellow and amino acids with post-translational modifications (PTM) are shown in green. Possible ubiquitination sites are highlighted with a red box.

i, Schematic diagram of domain structure of Clr4 protein and the position of lysine residues same as Fig. 1d but also shows possible ubiquitination sites characterized by Mass Spectrometry analysis on top.

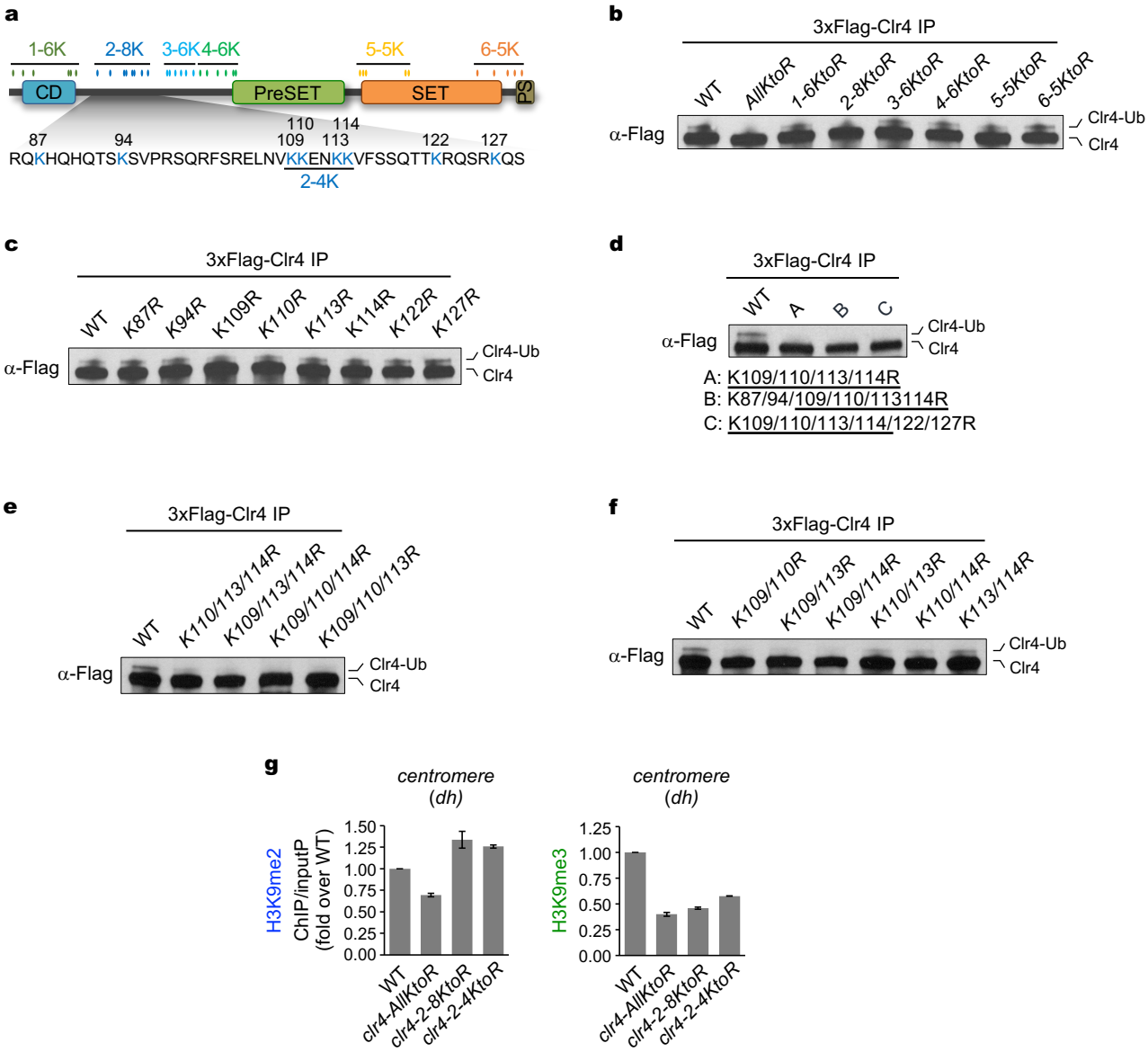

Extended Data Figure 6. Characterization of ubiquitination sites of Clr4 by genetic analysis.

a, Schematic diagram of domain structure of Clr4 protein and position of lysine residues, same as Fig. 1d.

b, Western blot (WB) analysis of immunoprecipitated 3xFlag-Clr4 from all-lysine mutant (*AllKtoR*) and 6 block mutants.

c-f, Western blot (WB) analysis of immunoprecipitated 3xFlag-Clr4 from 8 individual lysine to arginine mutants (**c**), 4 or 6 lysines to arginines mutants (**d**), triple combination of K109, K110, K113 and K114 to arginines mutants (**e**) or double combination of K109, K110, K113 and K114 to arginines mutants (**f**) of second block (2-8K) of Clr4.

g, ChIP-qPCR assays showing enrichment of H3K9me2 (left), H3K9me3 (right) at centromeric *dh* locus in the indicated strains. Error bars, S.D. (3 biological replicates).

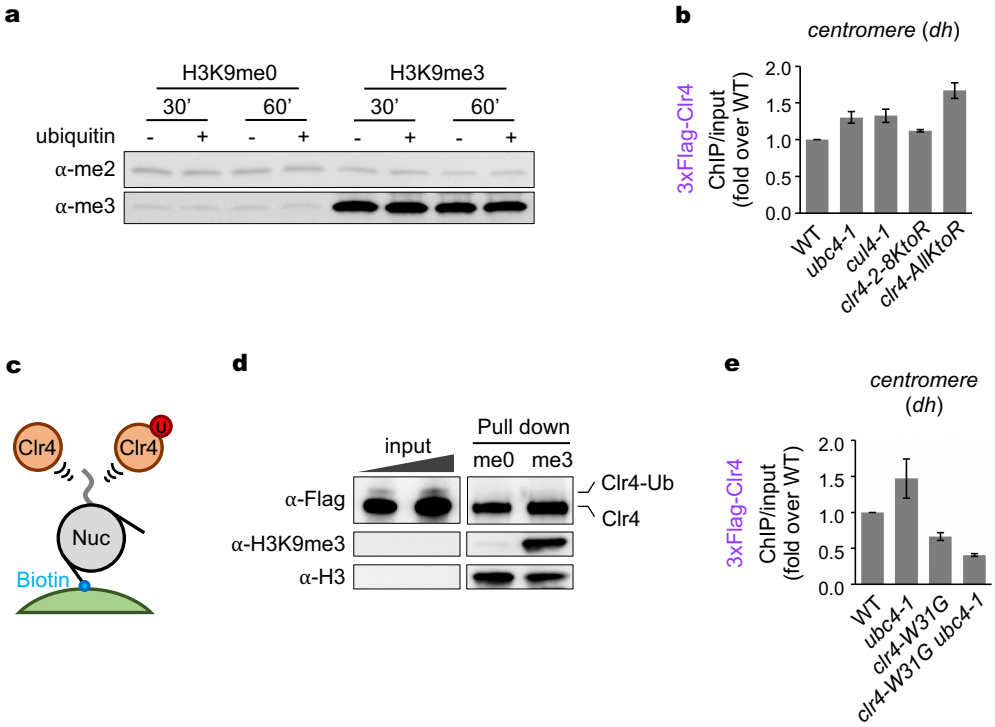

Extended Data Figure 7. Increased enrichment of Clr4 protein at centromeric heterochromatin in *ubc4-1, cul4-1*, second block mutant (*2-8KtoR*) and all-lysine mutant (*AllKtoR*).

a, Histone methylation assay. Nucleosomes with unmodified histone H3 (H3K9me0) or H3K9me3 histone (H3K9me3) were incubated with unmodified (ubiquitin, -) or *in vitro* ubiquitinated Clr4 proteins (ubiquitin, +) for the indicated times. Western blot (WB) analyses were carried out using H3K9me2 and H3K9me3 antibodies.

b, ChIP-qPCR assay showing enrichment of 3xFlag-Clr4 at centromeric *dh* locus in the indicated strains. Error bars, S.D. (3 biological replicates).

c, Schematic diagram for *in vitro* protein binding assay with nucleosomes. First, nucleosomes were anchored to Streptavidin beads using Biotin moiety at the end of DNA. Unmodified or ubiquitinated Clr4 proteins are added to reaction mixture and bound proteins were analyzed further by WB analyses.

d, *In vitro* protein binding assay of Clr4 protein from *S. pombe* cells with nucleosomes. 3xFlag-Clr4 purified from *S. pombe* cells were incubated with nucleosomes with unmodified histone H3 (me0) or H3K9me3 histone (me3) anchored to streptavidin beads. Input and precipitated proteins were analyzed by WB using antibodies as shown. Similar to the results of Fig. 2b, ubiquitinated Clr4 did not bind to the nucleosome.

e, ChIP-qPCR assay showing enrichment of 3xFlag-Clr4 at centromeric *dh* locus in the indicated strains. Error bars, S.D. (3 biological replicates).

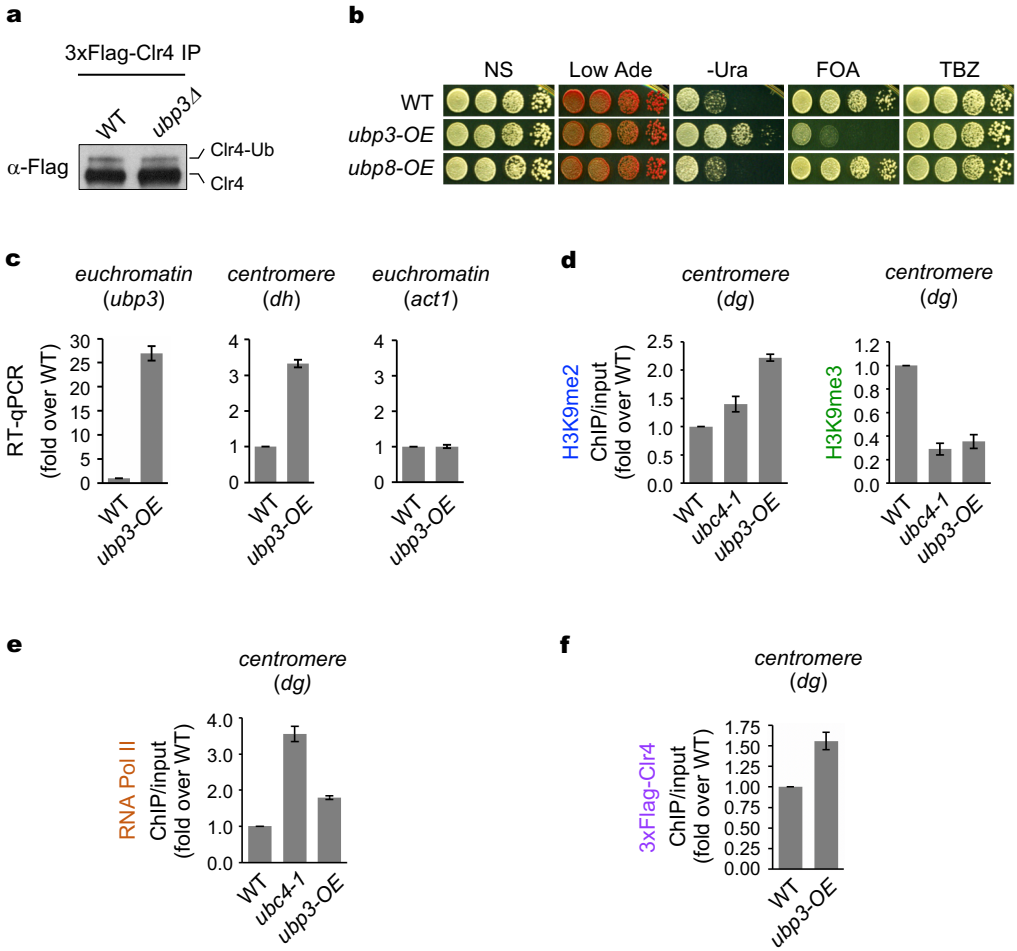

Extended Data Figure 8. The role of Ubp3 for de-ubiquitination of Clr4

a, Western blot (WB) analysis of immunoprecipitated 3xFlag-Clr4 shows that *ubp3* deletion does not cause clear change of Clr4 ubiquitination.

b, Silencing assay of centromeric *ade6*$^+$ gene (*otr1R::ade6*$^+$) on low-adenine (Low ade) and *ura4*$^+$ gene (*imr1L::ura4*$^+$) on no Uracil (-Ura) and 5'-fluroorotic acid (FOA) media for count selection of *ura4*$^+$ expression in Ubp3- or Ubp8-overexpression (-OE) cells. TBZ-sensitivity assay on media containing 15μg/ml thiabendazole (TBZ) media.

c. RT-qPCR analysis for *ubp3*, centromeric *dh* and *act1* transcripts in the indicated strains. Error bars, S.D. (3 biological replicates).

d, ChIP-qPCR assays show enrichment of H3K9me2 (left) and H3K9me3 (right) at centromeric *dg* locus in the indicated strains. Error bars, S.D. (3 biological replicates).

e, ChIP-qPCR assays showing enrichment of RNA Pol II (Rpb1) at centromeric *dg* locus in the indicated strains. Error bars, S.D. (3 biological replicates).

f, ChIP-qPCR assays show enrichment of 3xFlag-Clr4 at centromeric *dg* locus in the indicated strains. Error bars, S.D. (3 biological replicates).

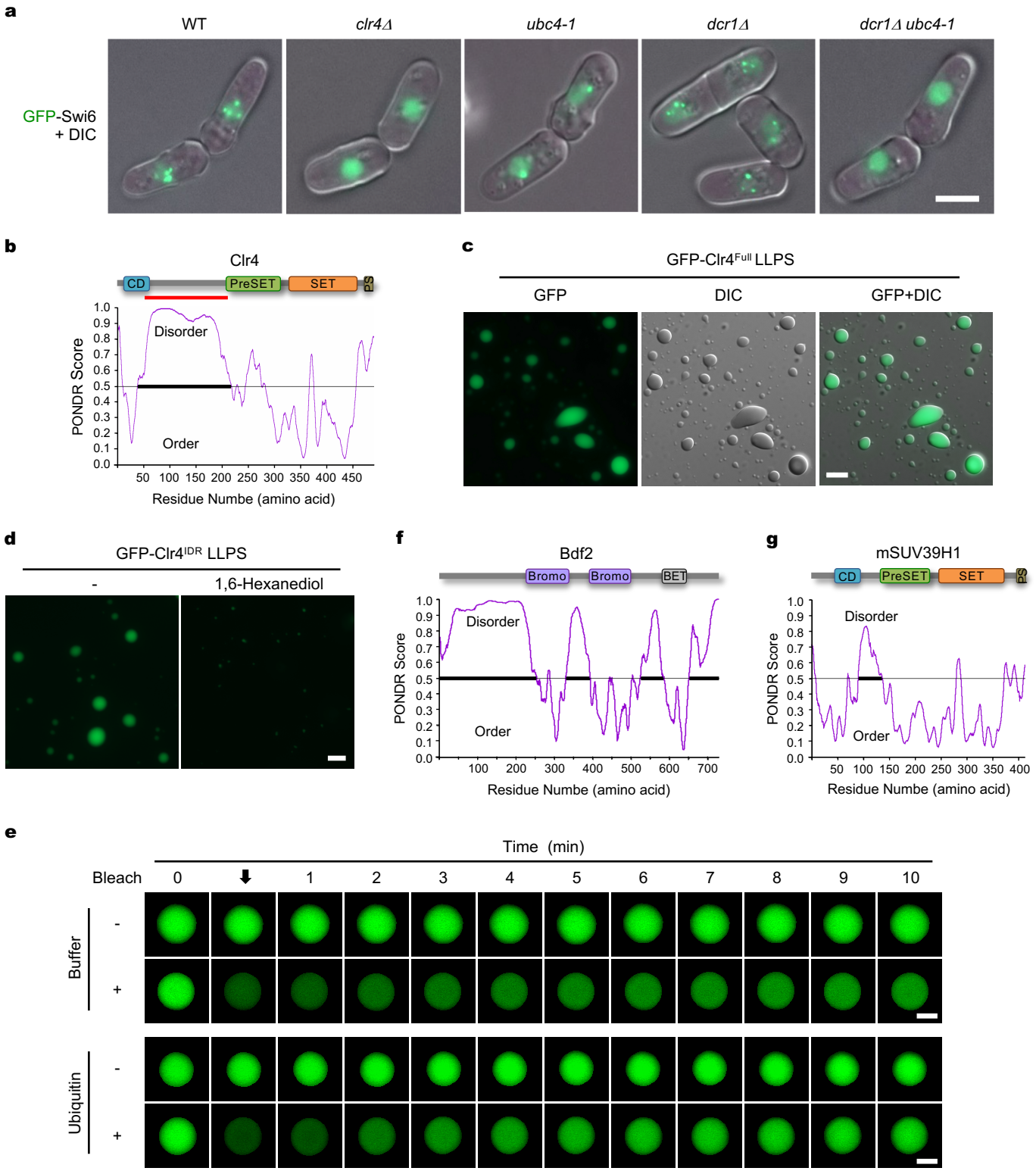

Extended Data Figure 9. LLPS of GFP-Clr4 proteins and disorder prediction

a. Live cell imaging showing the localization of GFP-Swi6 in indicated strains, same as Fig. 3a but showing GFP and DIC toghether. Scale bar, 2.5μm.

b, Schematic diagram of domain structure of Clr4 protein. Disorder prediction (PONDR) shows that the hinge region between chromodomain (CD) and PreSET of Clr4 is highly disordered. Red bar below the Clr4 schematic diagram shows the location of amino acids which is used for GFP-Clr4^{IDR} construct (51-220 amino acids).

c, LLPS of GFP-Clr4^{Full} protein. DIC; Differential interference contrast. Scale bar, 10μm.

d, The effect of 7.2% (w/v) 1,6-Hexanediol on LLPS of GFP-Clr4^{IDR} protein. Scale bar, 5μm.

e, FRAP of GFP-Clr4^{IDR} by addition of ubiquitin before and after bleaching. Representative droplests from Buffer and Ubiquitin with or without bleach were shown. Arrow shows the time of bleaching (~40s). Scale bar, 2μm

f, Schematic diagram of domain structure of Bdf2 protein (top). Disorder prediction (PONDR) shows that two Bromo and BET domains are ordered but the other regions are highly disordered.

g, Schematic diagram of domain structure of mouse SUV39H1 protein (top). Disorder prediction (PONDR) shows that the hinge region between chromodomain (CD) and PreSET of mSUV39H1 is highly disordered.

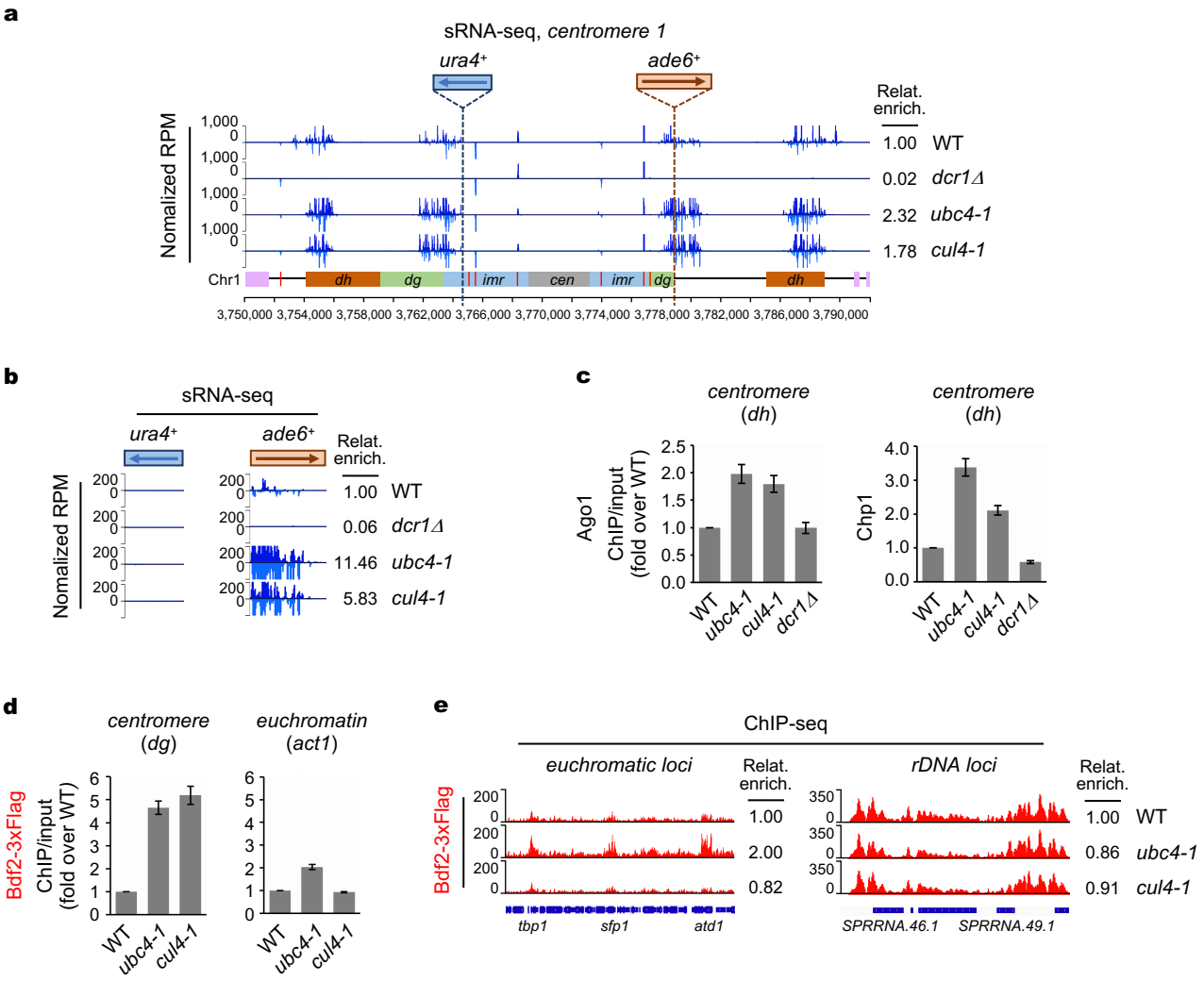

Extended Data Figure 10. Increased centromeric sRNA in *ubc4-1* and *cul4-1* mutants.

a, sRNA-seq reads mapped to chromosome 1 centromere. *ura4*$^+$ reporter gene is inserted in left *imr* (innermost repeats) just next to where sRNAs are produced. *ade6*$^+$ is located in right *otr* (outer repeats) where sRNA is hugely produced especially in *ubc4-1* and *cul4-1* mutants. Relat. enrich., relative enrichment of sRNA without tRNA.

b, Increased sRNA production at *ade6*$^+$ reporter gene in *ubc4-1* and *cul4-1* mutants but not at *ura4*$^+$. sRNA-seq reads of *ura4*$^+$ and *ade6*$^+$ reporter genes inserted at centromere 1 heterochromatin in the indicated strains. Relat. enrich., relative enrichment of sRNA.

c, ChIP-qPCR assays showing enrichment of Ago1 and Chp1 at centromeric *dh* locus in the indicated strains. Error bars, S.D. (3 biological replicates).

d, ChIP-qPCR assays showing enrichment of Bdf2-3xFlag at centromeric *dg* (left) and euchromatic *act1* (right) loci in the indicated strains. Error bars, S.D. (2 biological replicates).

e, ChIP-seq reads of Bdf2-3xFlag mapped to euchromatic loci on chromosome 1 right arm and rDNA loci on chromosome 3 right end in indicated strains. Relat. enrich., relative enrichment. Bottom, schematic diagram of chromosomal loci.